2019

Unraveling PDI and its Interaction with AB Toxins

Jessica Guyette
University of Central Florida

UNRAVELING PDI AND ITS INTERACTION WITH AB TOXINS

by

JESSICA LORRAINE GUYETTE
M.S. University of Central Florida, 2016
B.S. Worcester Polytechnic Institute of Technology, 2014

A dissertation submitted in partial fulfillment of the requirements
for the degree of Doctor of Philosophy
in the Burnett School of Biomedical Sciences
in the College of Medicine
at the University of Central Florida
Orlando, Florida

Summer Term
2019

Major Professor: Ken Teter

ABSTRACT

Protein disulfide isomerase (PDI) is an essential endoplasmic reticulum (ER) protein that acts as both an oxidoreductase and chaperone. It exhibits substantial flexibility and undergoes cycles of unfolding and refolding in its interaction with cholera toxin (Ctx), which is a unique property of PDI. This unfolding allows PDI to disassemble the Ctx holotoxin, which is required for Ctx activity. Here, we investigated the unfolding and refolding property of PDI and how this affects its interaction with bacterial toxins. PDI showed remarkable redox-linked conformational resilience that allows it to refold after being thermally stressed. Deletion constructs of PDI showed that both active domains play opposing roles in stability, and can both refold from an unfolded state, indicating that either domain could unfold during its interaction with Ctx. Its ability to refold suggests that the cycle of unfolding and refolding with Ctx is a normal mechanism that prevents protein aggregation. Disruption of this cycle with the polyphenol, quercetin-3-rutinoside, prevented the disassembly of Ctx, which blocked Ctx intoxication of cultured cells. Loss of PDI function was also found to inhibit intoxication with *Escherichia coli* heat-labile toxin but not with ricin and Shiga toxins. Toxin structure also contributes to efficiency of PDI binding and disassembly, which may explain the differential potencies between toxins. While Ctx and Ltx share similar structures, Ctx is more potent and efficiently disassembled compared to Ltx. We believe that PDI-mediated disassembly is the rate-limiting step in intoxication, thus dictating toxin potency. Overall, PDI can be targeted for a potential therapeutic for many bacterial toxins because of its unique unfolding properties and its key role in cell intoxication.

ACKNOWLEDGEMENTS

I would like to first and foremost thank Dr. Teter for his mentorship throughout my project, the guidance and constant support he's given me over the past 5 years, and for preparing me for my next step in my career. I would like to also thank my committee for supporting me and offering feedback that has greatly improved my project and expanded my knowledge in new areas. Specifically, I wanted to thank Dr. Tatulian for single-handedly teaching me everything I needed to know about biophysics and helping me analyze countless traces at all hours of the day. Lastly, I want to thank all the members in the lab for their patience with me, their determination to succeed, and their advice on experimental design.

TABLE OF CONTENTS

LIST OF FIGURES

LIST OF TABLES

LIST OF ACRONYMS & ABBREVIATIONS

cAMP: Cyclic adenosine monophosphate

CD: Circular dichroism

Ctx: Cholera toxin

CtxA1: Cholera toxin A1 subunit

CtxB: Cholera toxin B subunit

DMEM: Dulbecco's Modified Eagle Media

DTT: Dithiothreitol

ER: Endoplasmic reticulum

FTIR: Fourier-transform infrared spectroscopy

Gb3: Glycolipid globotriaosylceramide

GM1: monosialotetrahexosylganglioside

GSH: reduced glutathione

Ltx: Heat-labile toxin

MDH: Malate dehydrogenase

PDI: Protein disulfide isomerase

Q3R: Quercetin-3-rutinoside

RIU: Refractive index units

RIP: Ribosome-inactivating protein

Rtx: Ricin

SS: Signal sequence

STEC: Shiga toxin-producing *Escherichia coli*

SDS-PAGE: Sodium dodecyl sulfate polyacrylamide gel electrophoresis

Stx1: Shiga toxin 1

Stx2: Shiga toxin 2

SPR: Surface plasmon resonance

PBS: Phosphate buffered saline

PBST: Phosphate buffered saline Tween 20

TGN: *trans*-Golgi network

CHAPTER 1 INTRODUCTION

Many bacteria produce toxins as virulence factors that cause symptoms in patients and aid in their transmission to new hosts. These toxins are able to hijack normal cellular functions in order to generate a disease state. Protein disulfide isomerase (PDI), a host protein mainly located in the endoplasmic reticulum (ER), is linked to the cellular activities of many toxins. Understanding how PDI interacts with these toxins can open new opportunities for the development of anti-toxin therapeutics by targeting new functions of PDI.

1.1 Protein Disulfide Isomerase

PDI is an essential ER protein that promotes protein folding through both oxidoreductase and chaperone activity. It has a U-shaped **abb'xa'c** structure, with active -CGHC- sites in the **a** and **a'** domains, substrate binding **b** and **b'** domains, a flexible **x** linker region, and a short acidic **c** tail [1, 2]. The active cysteines in the **a** and **a'** domains can be oxidized or reduced, which causes a conformational change within the protein to allow an "open" conformation in the oxidized state or a "closed" conformation in the reduced state. In the open state, the **a'** arm of the protein is positioned out of plane from the rest of the protein, while the closed state has all domains of the U-shape in the same plane [3-5]. Changes in the redox state of PDI affect its substrate binding [3, 5-7] and functional properties as described below.

PDI is able to aid in protein folding by being an oxidoreductase in the ER. It is capable of creating, destroying, and rearranging disulfide bonds by its two redox states, oxidized and reduced PDI [8, 9]. PDI resides within the ER lumen, which is naturally an oxidizing environment [10]. When PDI acts on substrates to help fold unfolded or misfolded proteins, it obtains a free electron from its substrate which then reduces PDI. Once reduced, PDI can then

act on additional substrates in that state, such as AB toxins, or it can be converted back to its oxidized form by Ero1, which uses hydrogen peroxide as a substrate to act on PDI [11, 12]. PDI is constantly in a flux between the oxidized and reduced state, with a usual 3:1 ratio oxidized to reduced glutathione in the ER [10, 13] and 15% of ER-localized PDI in the oxidized state.

In addition to its oxidoreductase capabilities, PDI can also serve as a chaperone by binding to proteins to prevent aggregation. PDI is able to prevent the aggregation of proteins by binding and allowing the protein to naturally fold itself, rather than allowing misfolded proteins to aggregate [9]. Interestingly, we have discovered a new property of PDI which could be classified as a disaggregase activity, where PDI is able to unfold and refold its structure with specific substrates. This unfolding and refolding functionality has been observed with some AB toxins [14], but it could be a normal function for PDI to help break up protein aggregates in the cell. PDI has been shown to break apart aggregates of α-synuclein, which could aid in the prevention of amyloid plaques commonly found in patients with Parkinson's disease. Understanding how PDI is able to interact with its substrates can reveal valuable information on its functionalities and its potential use as a therapeutic.

1.2 AB Toxins

AB toxins are a group of bacterial and plant-derived toxins that contain a catalytic A subunit and a cell-binding B subunit [15, 16]. These toxins have the ability to bind to the cell surface and are internalized into the endosomes, where they can then translocate through different organelles to reach their cytosolic targets [17-20]. Some A subunits are proteolytically nicked, generating an A1/A2 disulfide-linked subunit. The catalytic A1 is anchored to the B subunit through the A2

linker. While an intact holotoxin is required for cellular entry, disassembly must occur to allow the free A or A1 subunit to reach the cytosol for a toxic effect [15, 20].

ER-translocating toxins use retrograde transport to move from the cell surface to the ER, where the toxin is reduced and disassembled. Once disassembled, the free A or A1 subunit spontaneously unfolds due to its thermal instability. This activates the ER-associated degradation pathway (ERAD), which exports unfolded or misfolded proteins from the ER to the cytosol where they are tagged with ubiquitin for future degradation by the proteasome. However, many ER-translocating toxins lack the lysine residues which are required for ubiquitination. As a result, these toxins evade degradation and are refolded in the cytosol using host chaperones.

PDI may play an active role in the reduction and disassembly of several ER-translocating toxins. The overall goal of this dissertation was to examine how the redox-dependent structural changes to PDI affect its interactions with five of these toxins: cholera toxin (Ctx), heat-labile toxin (Ltx), ricin (Rtx), Shiga toxin 1 (Stx1), and Shiga toxin 2 (Stx2). The next section will provide an overview of each toxin and its known link to PDI.

1.2.1 Cholera and Heat-Labile Toxins

Vibrio cholerae Ctx and *Escherichia coli* Ltx are ~80% homologous structurally, and they are both ER-translocating toxins that target the stimulatory α subunit of the heterotrimeric G protein on the cytoplasmic face of the plasma membrane [21, 22]. Both toxins are proteolytically nicked in either the bacterium (Ctx) or host (Ltx) to generate the A1/A2 subunits linked by a disulfide bond. Once they are disassembled and translocated into the cytosol, they are refolded into a catalytically active state and move to the plasma membrane, where they ADP-ribosylate Gsα [22]. This causes Gsα to constitutively activate adenylate cyclase, which then increases cAMP in

the cell and an efflux of water and chloride out of the cell. This process then causes watery diarrhea in patients which is treated with antibiotics (if they are available), rehydration of fluids, and supportive care [23, 24].

Although Ctx and Ltx both move through cells similarly, and they both have the same cytosolic target, it is well established that Ctx is more potent than Ltx in cells [17]. The disease state is more severe in patients with cholera intoxication and is more likely to cause fatalities among children and elderly patients as compared to those with enterotoxigenic *E. coli* infections [22]. Interestingly, however, LtxA1 is more catalytically active as compared to CtxA1, which begs the question: why Ctx is more potent than Ltx?

Since PDI can bind to many substrates, it is able to reduce AB toxins when they enter the ER if PDI is in the reduced state. Reduction of the toxin is essential for subsequent disassembly to occur because the catalytic portion of the AB toxins is disulfide-linked to the rest of the protein, which is too strong to be broken by a non-reductase protein-protein interaction.

Reduced Ctx will remain as an intact holotoxin that cannot translocate from the ER to the cytosol, and PDI has been shown to perform an additional step in order to disassemble Ctx [6, 7, 14, 25]. PDI unfolds upon binding to the holotoxin, which causes PDI to expand its hydrodynamic structure and act as a wedge to push the CtxA1 subunit away from the A2/B5 subunits. This force is capable of physically dislodging the CtxA1 subunit from the rest of the holotoxin, which allows the free A1 subunit to spontaneously unfold [6, 14, 26]. Once CtxA1 unfolds, PDI can no longer bind to it. Unfolded CtxA1 is then exported to the cytosol, where it is refolded into a catalytically active state by host factors. PDI is essential for the Ctx disassembly step, and cells lacking PDI are resistant to Ctx. After the interaction, PDI can then refold to its native structure, likely to be able to act on additional substrates. The work of this dissertation

adds new insight to PDI's interaction with Ltx, which is currently unknown, and the similarities between Ltx and Ctx during disassembly.

1.2.2 Ricin

Ricin toxin (Rtx) originates from *Ricinus communis*, also known as the castor oil plant, and can be extracted from the seeds. Rtx can be ingested, inhaled, or injected, and it is widely known as a bioterrorism threat because of its potency and ease of weaponization. Once intoxicated, the patient can have a variety of symptoms based on the mode of entry into the body, which can start over the course of a few hours to a few days depending on the dose. Symptoms include nausea, diarrhea, fever, coughing, vomiting, and hemorrhaging. If treatment is not begun immediately after contact with Rtx, the intoxication could be fatal or severely damaging. Treatment for Rtx intoxication is mainly supportive care, although new studies are using neutralizing monoclonal antibodies to scavenge ricin before it can be internalized by cells [27]**.**

Rtx is a lectin with a catalytic A subunit and a cell-binding B subunit synthesized as a single protein, nicked in the plant to generate a disulfide-linked, AB holotoxin [20, 28, 29]. Rtx binds terminal galactose residues on cells and is internalized into the endosomes. From here, it uses retrograde transport to move from the endosomes, through the Golgi, and into the ER [30]. Once in the ER, it is reduced and disassembled to allow the free A subunit to be exported into the cytosol, where it can reach its cytosolic target, the ribosomes. RtxA is a ribosome-inactivating protein (RIP), and it inactivates the 28S rRNA of the ribosome by utilizing an N-glycosidase activity, which cleaves the rRNA at an adenine residue, thus preventing the ribosome from making new proteins [15, 19]. Disruption of enough ribosomes causes a halt in protein synthesis and will eventually lead to cell death [15].

PDI can reduce the disulfide bond in Rtx [31]. However, other oxidoreductases are also capable of reducing the disulfide bond [20]. Interestingly, the link between reduction and disassembly for Rtx has not been studied, and it is unknown if reduction and disassembly are coupled events for Rtx.

1.2.3 Shiga Toxins

Shiga toxin (Stx) is an RIP produced by *Shigella dysenteriae* [32]. However, similar toxins known as Shiga-like toxins are produced by *Escherichia coli* as a result of lysogenic conversion [29]. There are 2 main types of Shiga-like toxin, Shiga toxin 1 (Stx1) and Shiga toxin 2 (Stx2). Stx1 is the most homologous to the original Stx, with only 1 amino acid change, while Stx1 and Stx2 share about 56% sequence homology [31]. Stx1 and Stx2 are generally transmitted through Shiga toxin-producing *E. coli* (STEC), which is found on unwashed or under-cooked foods. Outbreaks of STEC have been more common recently, with batches of contaminated lettuce and other produce causing disease throughout the United States. Symptoms of an STEC infection are similar to ricin intoxication, with nausea, vomiting, and diarrhea. Kidney failure can occur if not treated [28]. Antibiotics, unfortunately, cannot be used to treat STEC infections because the phage SOS response and lysis of the bacteria release a significant volume of Stx into the gut, causing even more severe symptoms and can be fatal.

Stxs contain a similar structural setup as compared to Ctx and Ltx, with a catalytic A1 subunit disulfide-linked to an A2 linker which extends into a B pentamer. Stx binds to glycolipid globotriaosylceramide (Gb3) on the cell surface which it uses to be internalized into the endosomes [17]. Similarly to Ltx, Stx is nicked by the host protease furin to generate the A1/A2 linked subunits. Nicked Stx enters the ER for reduction and disassembly, but the role that PDI

plays during Stx reduction and disassembly is currently unknown. After disassembly, the free A1 subunit translocates to the cytosol where it kills the cell by halting protein synthesis through a mechanism identical to the catalytic activity of RtxA.

1.3 Summary

Overall, this project analyzed PDI's interaction with multiple AB toxins to elucidate which toxins require PDI for intoxication, and which function of PDI (oxidoreductase, chaperone, or disaggregase) is involved with this process. We have determined a main structural difference between two similar toxins, Ctx and Ltx, and how their interaction with PDI dictates toxin potency. In addition, we have determined the mechanism of action for a novel PDI inhibitor, which can further be used as an anti-toxin therapeutic. Lastly, the structural mechanism of PDI's unfolding abilities have been investigated. This collective work has provided new insight on the structure and function of PDI and its role in the potency of AB toxins.

CHAPTER 2 REDUCTION IS SUFFICIENT FOR HOLOTOXIN DISASSEMBLY OF RICIN BUT NOT *ESCHERICHIA COLI* HEAT-LABILE TOXIN

2.1 Introduction

AB toxins are a family of bacterial and plant-derived proteins that contain a catalytic "A" subunit and cell-binding "B" subunit [15, 16]. These toxins all bind to the cell surface through individual receptors and are internalized into the endosome. From here, the toxins use retrograde transport to move from the endosomes to other organelles for further processing and subsequent disassembly [17-20]. Disassembly is essential for cell intoxication because it allows separation of the catalytic A subunit from the holotoxin, which is then free to reach its target and induce cytotoxicity.

For many ER-translocating toxins, a disulfide bond connects the catalytic subunit to the rest of the toxin. This disulfide can be direct, as per ricin (Fig 2.1A), which connects the A and the B subunits, or it can involve an A2 linker that is produced from a precursor A chain [15, 20]. Some A chains can be proteolytically nicked to generate an A1/A2 heterodimer, where the catalytically active A1 subunit is disulfide-linked to the A2 linker, which extends into the central pore of the B pentamer. *Vibrio cholerae's* cholera toxin (Ctx, Fig 2.1B) and *Escherichia coli's* heat-labile toxin (Ltx, Fig 2.1C) are ~80% homologous, and both have an α-helical A2 linker that extends into the B pentamer [22]. Similarly, Shiga toxin 1 (Stx1, Fig 2.1D) and Shiga toxin 2 (Stx2, Fig 2.1E), which are ~55% homologous, contain a less structured A2 linker that also extends into the B pentamer pore [17, 31, 32].

Reduction and disassembly appear to be coupled events for some ER-translocating toxins but not others. Removal of the cysteines that create the disulfide bond between StxA1 and A2 resulted in

a disassembled toxin, suggesting that nicking and reduction of the holotoxin is sufficient for toxin disassembly [33]. Although it has been shown that various oxidoreductases (or factors) can reduce the Rtx disulfide bond, subsequent disassembly was not examined [20]. In contrast, reduced Ctx remains as an intact holotoxin, and it requires protein disulfide isomerase (PDI) for toxin disassembly [6, 7, 14, 25]. PDI is an essential ER oxidoreductase and chaperone that, upon binding to Ctx, expands its structure and acts as a wedge to physically dislodge CtxA1 from the rest of the holotoxin [14]. It is unknown if other AB toxins require PDI and its unfolding mechanism for disassembly, or if reduction alone can disassemble holotoxins.

Here, we show that reduction alone can disassemble Rtx, Stx1, and Stx2 but not Ltx, and for the first time, reduction and disassembly are coupled events for these toxins. Conversely, disassembly of Ltx required the presence of PDI, which was required for Ltx intoxication of cultured cells. Together, these data provide insight into the reduction and disassembly of ER-translocating AB toxins and how PDI interacts with various toxin structures.

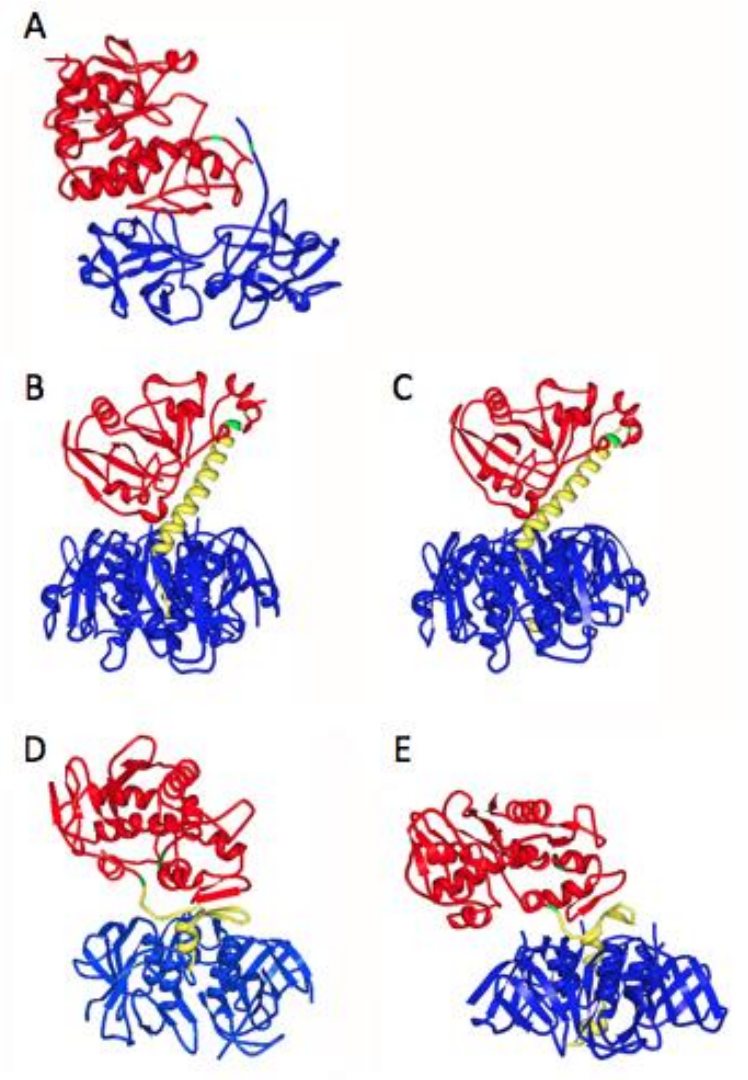

Figure 2.1: Ribbon diagrams of AB toxins

Ribbon diagrams of Rtx (A- PDB: 2AAI), Ctx (B- PDB: 1S5F), Ltx (C- PDB: 1LTS), Stx1 (D- PDB: 1DM0), and Stx2 (E- PDB: 1R4P). Catalytic A/A1 subunits (red) are disulfide linked (green) to either the A2 linker (yellow) or directly to the B subunit (blue).

2.2 Methods

2.2.1 Toxicity Assays

Parental TZM and PDI-deficient TZM cells obtained from Dr. Joel Silver (National Institutes of Health, Bethesda MD) were grown to ~85% confluency in 24-well plates and challenged with toxin the day after seeding. PDI-deficient cells were stably transfected with a siRNA construct that knocked down PDI to approximately 18% of wild-type expression levels. Cell intoxication involved exposure to Ltx, Rtx, Stx1, or Stx2 in serum-free DMEM for 18 h.

After Ltx treatment, the intoxicated cells were washed three times with PBS before the addition of ice-cold acidic ethanol (HCl:EtOH at a 1:99 ratio) for 15 min at 4°C. Cell extracts were then collected and allowed to evaporate overnight. The samples were subsequently reconstituted in buffer and analyzed for cAMP using the BioTek Enzyme Immunoassay System as per manufacturer's instructions (GE Healthcare, Chicago, IL). Data were collected from a BioTek plate reader. Basal cAMP levels from unintoxicated cells were background subtracted from toxin-treated cells, and final data were calculated as percentages of our maximal cAMP signal, which was intoxication of parental TZM cells with 100 ng/mL of Ltx.

After treatment with Rtx, Stx1, or Stx2, the intoxicated cells were starved in 500 µL of methionine-free medium for 30 min before supplementation of the medium with 5 µCi of [^{35}S] methionine for an additional 30 min. The cells were then exposed to ice-cold 10% TCA in PBS for sequential 30 and 10 min incubations. Cell lysates generated with 0.2 N NaOH were collected and placed in Ecoscint scintillation fluid (National Diagnostics, Atlanta, GA) for measurement with a BeckmanCoulter (Indianapolis, IN) LS6500 multi-purpose scintillation

counter. Final data were calculated as percentages of our maximal protein synthesis signal from unintoxicated cells. Both toxin treatments had 3 replicates per sample in a 24-well plate.

2.2.2 Rtx reduction

Rtx (2 μg in 10 μL 1x PBS) was incubated with varying concentrations of reduced glutathione (GSH) and equimolar amounts of oxidoreductases as indicated. After 30 min at 37°C, 5 μL of 4x sample buffer was added. The samples were boiled for 5 min, resolved by non-reducing sodium dodecyl sulfate-polyacrylamide gel electrophoresis (SDS-PAGE) with 15% polyacrylamide gels, and visualized using Coomassie stain.

2.2.3 Ltx nicking

50 ng Ltx was nicked with 1 μg of trypsin in a total volume of 10 μL 1x PBS for 30 min at room temperature before the addition of 1 μg trypsin soybean inhibitor and 5 μL of 4x sample buffer. Ltx samples were then resolved by non-reducing SDS-PAGE with 15% polyacrylamide gels, transferred to a PDVF membrane, blocked in 4% milk for 30 min, and processed for Western blot. The membrane was then incubated at 4°C overnight with rabbit-anti cholera toxin antibody (1:5,000 dilution, Sigma) and a 1 h room temperature incubation with the HRP-conjugated goat anti-rabbit IgG secondary antibody (1:10,000 dilution).

2.2.4 Surface plasmon resonance (SPR)

For Ltx, 100 μL of ethanol containing 500 ng GM1 (Fisher Scientific, Waltham, MA) was placed on a gold plate (Reichert, Dewpew, NY) and allowed to evaporate overnight. The GM1-coated plate was set in the Reichert SR7000DC refractometer and exposed to 1x PBS with 0.1%

Tween 20 (PBS-T) perfusion buffer containing 400 ng/mL of pre-nicked Ltx for 3 min at a flow rate of 41 µL/min for all steps. A baseline measurement (0 RIU) corresponding to the mass of the nicked Ltx holotoxin was then recorded. The experiment was initiated by perfusion of GSH or various oxidoreductases (0.3 µg/mL) over the plate. Oxidoreductases for were pre-reduced with 10 mM GSH for 30 min at room temperature before dialyzing in 1 L PBS with 3- 1 hr exchanges. After removal of GSH or oxidoreductase from the PBST perfusion buffer, the 35C2 monoclonal antibody against CtxA1 (1:100 dilution) and a polyclonal antibody against CtxB (1:1,000 dilution) were sequentially added to the perfusion chamber for detection of LtxA1 and LtxB.

For Rtx, activated monolayer plates (Reichert) were coated with asialofetuin type 2 (Sigma, 0.2 mg/mL) by perfusing it over the plate for 3 min. Asialofetuin type 2 has a terminal galactose residue that allows RtxB binding [28]. The plate was subsequently blocked with a 3 min exposure to PBST perfusion buffer containing 1 M ethanolamine (pH 8.5), and Rtx (0.6 µg/mL) was captured on the plate through a 3 min perfusion in PBST. A baseline measurement corresponding to the mass of the bound Rtx holotoxin (0 RIU) was recorded. The experiment was then initiated by perfusion of GSH or various oxidoreductases (0.3 µg/mL) over the plate. After removal of GSH or oxidoreductase from the PBST perfusion buffer at 180 sec post-injection, polyclonal antibodies against RtxA and RtxB (each used at 1:1,000 dilutions, BEI Resources, Manassas, VA) were sequentially added to the perfusion chamber. Final data were processed with Scrubber (BioLogic Software, Canberra, Australia) and final images were produced in Igor (Wavemetrics, Portland, OR).

2.2.5 ^{13}C-labeled and non-labeled protein purification

Starter cultures in 5 mL of Luria broth with 100 μg/mL ampicillin were grown overnight, expanded to 1 L cultures, and induced at an O.D. of 0.6 with 1 mM ITPG for 4 h at 37°C. Induced cultures were spun for 20 min at 6,000 rpm and 4°C before freezing the cell pellet at -80°C. Pellets were resuspended in lysis buffer (100 μg/mL lysozyme; 1% deoxycholate; 0.1% Triton X-100; 20 mM sodium phosphate buffer pH 7.0; 300 mM sodium chloride) and subjected to sonication. The cell lysate was spun at 12,000 x g for 30 min at 4°C.

TALON beads (Clontech, Mountain View, CA) were washed three times with extraction buffer (20 mM sodium phosphate buffer pH 7.0; 300 mM sodium chloride) and spun down for 2 min at 700 x g. Once washed, the sonicated, clarified cell lysate was added to the beads and rotated overnight at 4°C. The PDI-bound beads were then washed 3 times in wash buffer (20 mM sodium phosphate buffer pH 7.0; 600 mM sodium chloride; 0.1% Triton X-100) for 15 min each while rotating at room temperature. Washed beads were added to a 2 mL TALON Gravity Column (Clontech), and extraction buffer was added to allow the column to pack. PDI was then eluted from the packed beads using extraction buffer containing 10, 20, 40, 60, or 100 mM imidazole. Fractions were run on an SDS-PAGE gel to ensure purity. PDI-containing fractions were then pooled, loaded into a 20,000 MWCO Slide-A-Lyzer Dialysis Cassette (Thermo Fisher Scientific, Waltham, MA), and dialyzed with three 1 h exchanges in 1 L pure water. Protein concentration was calculated using the Pierce BCA Protein Assay Kit (Thermo Fisher Scientific). Purified protein was then aliquoted into 100 μg samples and allowed to freeze overnight at -80°C before lyophilization.

For the production of uniformly ^{13}C-labeled PDI, ^{13}C-D-glucose (Cambridge Isotope Laboratories, Cambridge, MA) was used as the sole carbon source in M9 minimal medium.

Cultures were pelleted, and protein was purified by TALON affinity chromatography as previously described. To confirm the purity of each construct, SDS-PAGE with Coomassie blue stain was used to visualize a 2 µg sample of each protein. Aliquots (50 µg) of each protein were then frozen overnight at -80°C before lyophilization.

2.3 Results

2.3.1 Impact of PDI on cellular activity of AB toxins

To determine which toxins require PDI for their cellular activity, parental and PDI-deficient cells were intoxicated with various AB toxins and either protein synthesis or cAMP levels were monitored (Fig 2.2) with the help of David Curtis. Parental cells intoxicated with Ltx showed an increase of cAMP as the toxin concentrations increased. However, cAMP levels were minimal in the PDI-deficient cells at all toxin concentrations, indicating that these cells were resistant to intoxication (Fig 2.2A). Conversely, when PDI-deficient cells were intoxicated with either Rtx (Fig 2.2A), Stx1 (Fig 2.2C), or Stx2 (Fig 2.2D), all toxins were able to induce cytotoxicity and decrease protein synthesis over a range of toxin concentrations. Interestingly, the PDI-deficient cells proved to be more sensitive to Rtx and the Stxs as compared to intoxication of the parental cells. Together, these data show that PDI is essential for Ltx intoxication, but dispensible for intoxication with Rtx, Stx1, or Stx2.

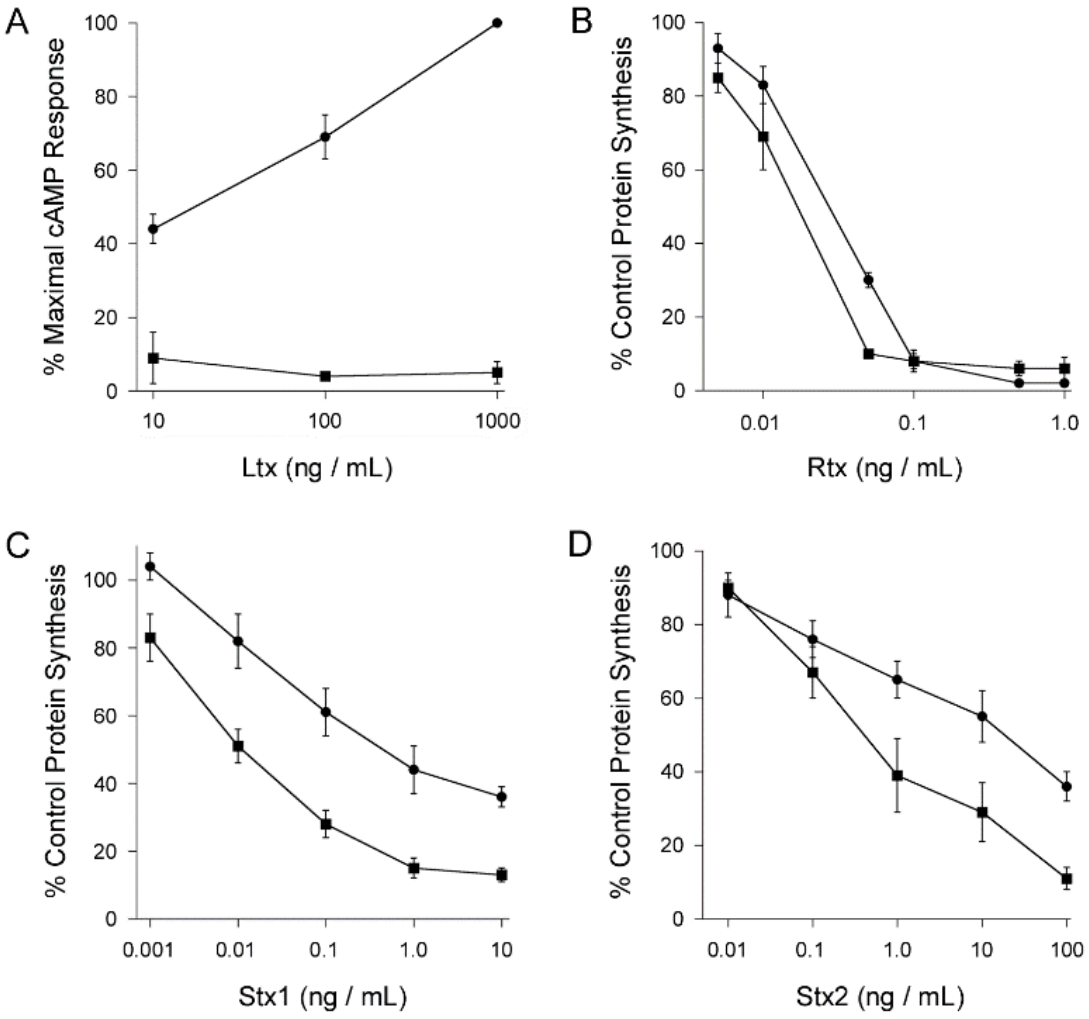

Figure 2.2: Toxin activity against PDI-deficient cells

TZM (circles) and PDI-deficient (squares) cells were intoxicated with increasing concentrations of toxin and were either processed for cAMP output (A) or protein synthesis (B-D). Background-subtracted cAMP data were expressed as percentages of the maximal signal, which was intoxicated cells at the highest concentration. Error bars are representative of standard error of the mean with an n= 4.

2.3.2 Reduction of Rtx

Since PDI is not required for Rtx intoxication, other oxidoreductases or reductants could be responsible for the reduction and disassembly of Rtx. To examine this possibility, we first incubated Rtx with increasing concentrations of reduced glutathione (GSH) to reduce the disulfide bond in Rtx (Fig 2.3) and observed the shift from a disulfide linked toxin to the monomeric A and B subunits by non-reducing SDS-PAGE. As shown in Fig 2.3A, 1 mM GSH was able to partially reduce the Rtx holotoxin and 5 mM GSH was able to fully reduce the disulfide bond. The oxidoreductases PDI, ERp57, and ERp72 were all capable of reducing the Rtx holotoxin as well (Fig 2.3B). To demonstrate that not all proteins are capable of reducing Rtx, the toxin was also incubated with lysozyme and 1 mM GSH. Under this condition, reduction beyond was what observed with GSH alone was not observed (Fig 2.3C). These data show that Rtx can be reduced by strong reductants or several ER resident oxidoreductases, and PDI is not essential for this step in Rtx intoxication. Thus, consistent with the toxicity data (Fig 2.2B), the reduction of Rtx is not dependent upon PDI.

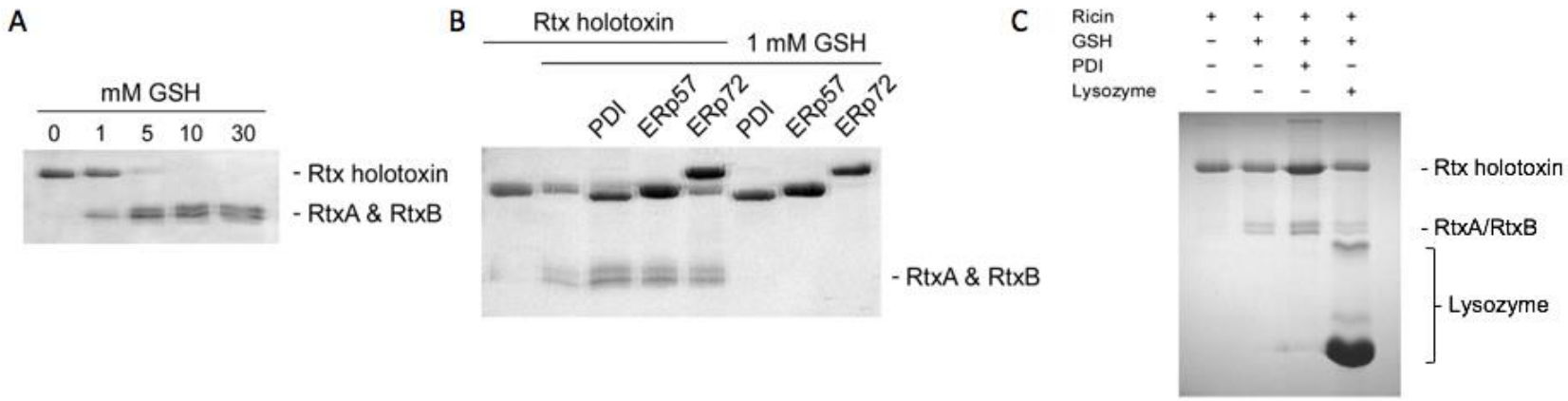

Figure 2.3: Reduction of Rtx

Non-reducing SDS-PAGE with Coomassie stain was used to resolve samples of Rtx that had been exposed to increasing concentrations of GSH (A) or with 1 mM GSH and various ER oxidoreductases (B) or lysozyme as a negative control (C). Reduction of the Rtx disulfide bond resulted in a doublet of ~30 kDa RtxA and RtxB bands.

2.3.3 Effect of reduction on the disassembly of Rtx

We and others have shown that reduction of Rtx can occur by various conditions [20], however, it was unknown if reduction alone leads to holotoxin disassembly. To observe the disassembly of Rtx in real time, SPR was used (with the help of Dr. Mike Taylor) to determine if reduction and disassembly were coupled events. With SPR, a ligand-bound sensor slide is exposed to an analyte in a perfusion buffer. Addition or subtraction of mass to the slide, indicating binding of substrates or loss of ligand, respectively, is detected by a change of signal in real time. Rtx holotoxin was appended to a sensor slide through an asialofetuin type 2 receptor and baselined to 0 refractive index units (RIU). 10 mM GSH (Fig 2.4A), PDI (Fig 2.4B), or ERp72 (Fig 2.4C) were perfused over the toxin in a perfusion chamber to observe a potential change of mass. Following the perfusion, Rtx antibodies for both the A and B subunits were sequentially perfused over the slide to indicate which subunits were still bound to the slide. If Rtx remained as an intact holotoxin and both subunits were present, both antibody controls would show a positive signal. However, the antibody control would produce no change in RIU signal when the subunit was absent or removed. GSH perfusion resulted in the removal of mass from the slide, with subsequent perfusions of the antibody controls indicating that the Rtx A chain was removed (Fig 2.4A). PDI (Fig 2.4B) and ERp72 (Fig 2.4C) showed binding to the Rtx-coated sensor slide as indicated by an increase in RIU. Upon removal of the oxidoreductase from the perfusion buffer, the RIU decreased below the initial baseline of the intact Rtx holotoxin. Antibody controls showed that RtxA was removed from the slide, confirming toxin disassembly. To demonstrate both antibodies recognize their cognate subunits in the Rtx holotoxin, we recorded increased RIU signals with either anti-RtxA or anti-RtxB antibodies that were perfused over a slide containing

the Rtx holotoxin (Fig 2.4D). These experiments demonstrate that reduction alone is sufficient for Rtx disassembly, and this can be achieved either by GSH or various oxidoreductases.

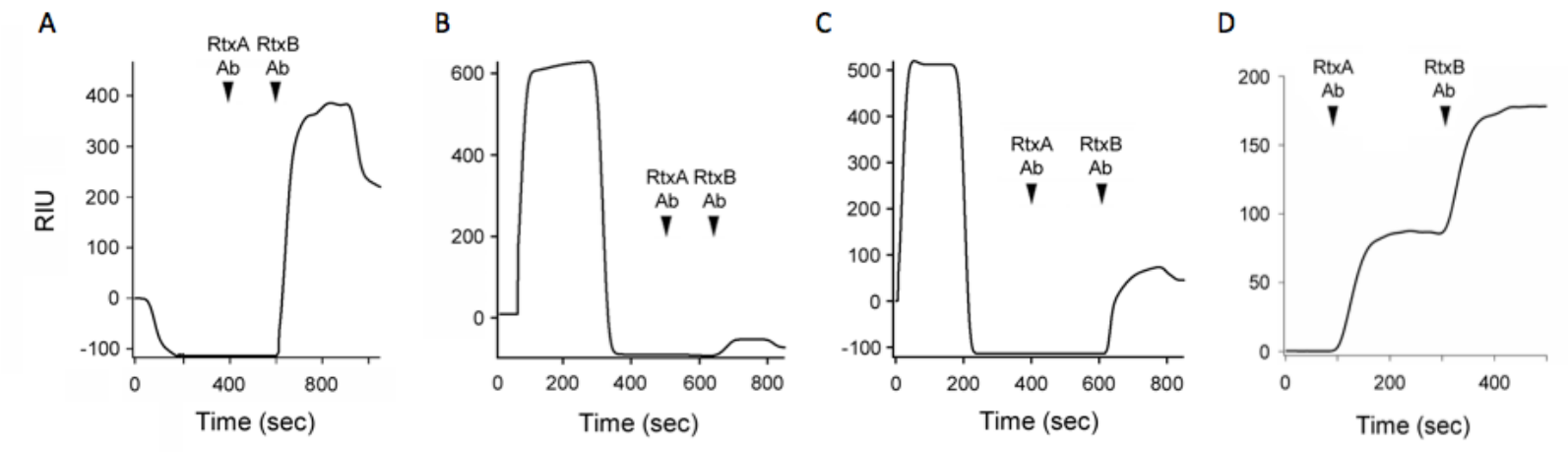

Figure 2.4: Real-time disassembly of Rtx

Rtx holotoxin was captured on a SPR sensor slide coated with asialofetuin type 2. The mass of the receptor-toxin complex was then baselined to 0 RIU. 10 mM GSH (A), reduced PDI (B), reduced ERp72 (C), or PBS-T (D) were perfused over the slides and removed from the perfusion buffer. Antibody controls for RtxA and RtxB were perfused over the slide (as indicated by the arrowheads) for 3 min each to determine if disassembly occurred.

2.3.4 Nicking and reduction of Ltx

LtxA is nicked by host proteases in the endosomes and/or *trans*-Golgi network (TGN) [22] to generate A1 and A2 subunits, which are connected by a disulfide bond (Fig 2.1B). Nicking of the A subunit is essential for subsequent toxin disassembly and toxin activity [22]. We simulated this nicking event with an established *in vitro* method by incubating Ltx from a commercial vendor with trypsin to generate the separate A1 and A2 subunits. The products were then analyzed by non-reducing SDS-PAGE (Fig 2.5). Interestingly, we found that the holotoxin was already reduced, and, upon nicking, we saw a reduced band for LtxA1 rather than the higher molecular weight band for disulfide-linked A1/A2 subunits. It thus appears that the commercially produced toxin was reduced during preparation. However, this same toxin was still intact and functional for the previously described cell intoxication assays (Fig 2.2A). This indicates that reduction alone does not cause disassembly for Ltx. Otherwise, our purchased Ltx would disassemble after the endosome/TGN nicking process, which would prevent LtxA1 transport to the ER and cytosol. In addition, these data indicate that PDI is performing an essential role in Ltx intoxication other than reduction of the disulfide bond, since Ltx was already reduced (Fig 2.1A).

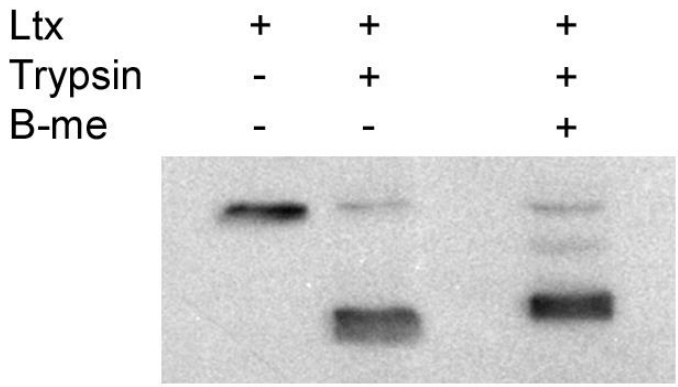

Figure 2.5: Ltx nicking and reduction

Various combinations of Ltx, trypsin, and β-mercaptoethanol were incubated at room temperature for 30 min before analysis with non-reducing SDS-PAGE and Western blot.

2.3.5 Effect of oxidoreductases on the disassembly of Ltx

Similarly to Rtx (Fig 2.4), we used SPR to determine which conditions are capable of disassembling the Ltx holotoxin. A SPR sensor slide was coated with the GM1 ganglioside receptor for Ltx, trypsin-nicked Ltx was captured on the plate, and the RIU was baselined to 0 signal representing the mass of the Ltx holotoxin. 10 mM GSH (Fig 2.6A), PDI (Fig 2.6B), and ERp72 (Fig 2.6C) were then perfused over the holotoxin-coated sensor. The addition of GSH did not cause a change in the overall mass on the slide, and antibody controls confirmed that an intact holotoxin remained bound (Fig 2.6A). Thus, GSH alone did not remove the A1 subunit from the already reduced holotoxin. This confirmed reduction alone does not cause disassembly of nicked Ltx. Conversely, PDI was able to remove the A1 subunit from the rest of the holotoxin (Fig 2.6B). Addition of PDI caused an increase of mass on the slide, indicating binding of PDI to Ltx. Only the A2/B_5 complex was left on the plate at the end of the experiment, as confirmed by antibody controls that detected the B pentamer but not PDI or LTA1 (Fig 2.6C). While ERp72 was not able to disassemble the toxin, it still showed binding to the toxin (Fig 2.6C). Upon perfusion over the slide, ERp72 caused an increase in signal indicating that it bound to Ltx. Removal of ERp72 from the perfusion buffer caused the signal to drop back to the baseline value of the Ltx holotoxin, and antibody controls showed that both Ltx subunits were still present on the slide. This indicated that binding and reduction alone were not sufficient for Ltx disassembly. Instead, PDI specifically is needed for Ltx disassembly to occur, demonstrating that it is performing an additional function that cannot be done by either reductant alone or ERp72. As shown by our intoxication assays (Fig 2.2A), this functionality is essential for subsequent toxin activity.

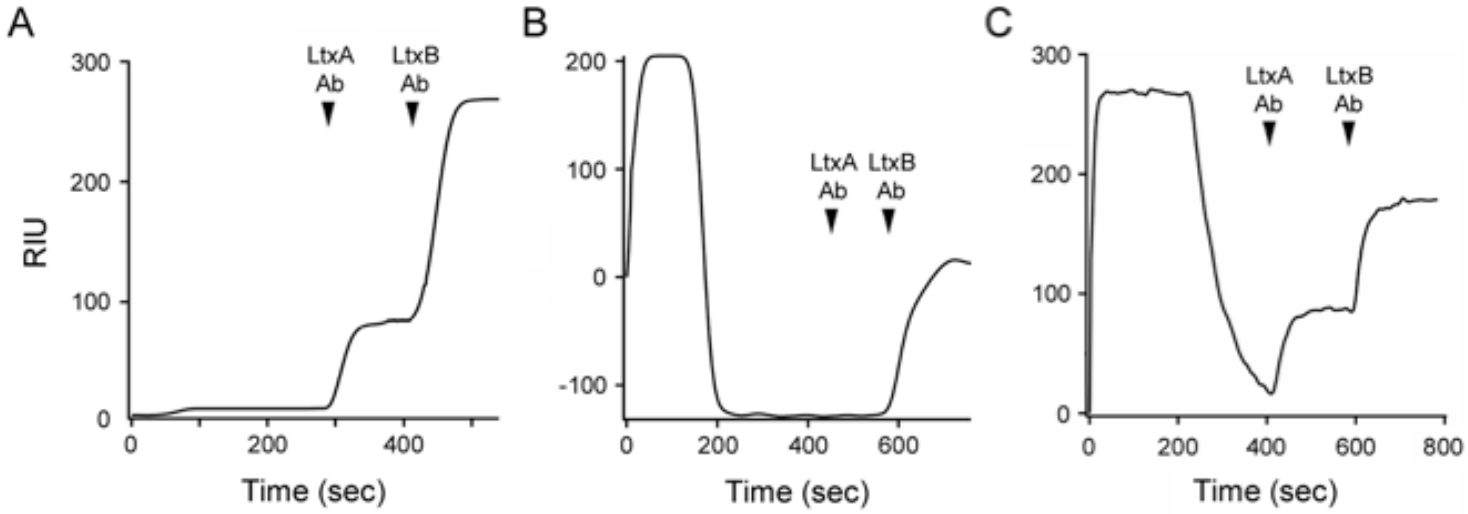

Figure 2.6: Real-time disassembly of Ltx

GM1-coated sensor slides were used to capture Ltx and baselined to 0 RIU before the start of the experiment. 10 mM GSH (A), reduced PDI (B), or reduced ERp72 (C) were perfused over the slides and removed from the perfusion buffer. Antibody controls for LtxA and LtxB were perfused over the slide (as indicated by the arrowheads) to determine if disassembly occurred.

2.4 Discussion

These data provide insight into the reduction and disassembly events of two AB toxins, Rtx and Ltx. We have shown that these events are coupled for Rtx but not Ltx. It has been previously noted that reduction and disassembly are coupled events for Stx [29]. Although many oxidoreductases have been shown to reduce the Rtx disulfide bond, reduction has not been shown to lead to Rtx disassembly until now.

Ctx can be reduced when entering the ER [34], yet, only PDI is capable of its subsequent disassembly by its unique unfolding capabilities [14]. We found that a similar toxin, Ltx, also required PDI for its disassembly and that reduction of the disulfide bond alone did not allow separation of the nicked A1 and A2/B_5 subunits. Ctx and Ltx share ~80% homology, and both contain structurally compact structures as compared to Stxs and Rtx (Fig 2.1). Although Stx1 and Stx2 share a similar A2 linker with Ctx and Ltx, the later toxins contain a close contact between the A1 and A2 linker subunits, which could be stabilizing the overall holotoxin even when the disulfide bond is reduced. Stx1, Stx2, and even Rtx have more expanded structures, where the A1 or A subunits are more distant from the A2 or B subunits, which could allow immediate dissociation during reduction.

We have shown that Ctx [14] and now Ltx both require PDI for toxin disassembly. This is due to the ability of PDI to unfold and act as a wedge to physically push apart the holotoxin. We hypothesize that PDI is not unfolding in the presence of Rtx or Stxs, since reduction and disassembly are linked for both toxins, and thus the unfolding of PDI would be unnecessary to ensure disassembly. Future experiments would test this hypothesis by observing any conformational changes in PDI during interactions with these toxins. The Teter lab has found

that PDI also unfolds upon contact with α-synuclein but not malate dehydrogenase (MDH). While the mechanism of when PDI unfolds upon substrate contact is still unknown, it could be linked to where the substrate is binding to PDI.

It is important to note that the unfolding property of PDI has not been seen with other common substrates such as malate dehydrogenase and insulin, which bind to PDI in the **b'** domain. Although it is currently unknown where Ctx and other AB toxins bind to PDI, it could be possible that they are binding to the **b** domain, which could induce unfolding and explain why PDI's unfolding property has not been observed previously. We hypothesize that binding to the **b** domain sends a signal through **b'x** to cause unfolding of the **a'** domain, which acts as a wedge to physically disassemble the toxin.

Since PDI is required for Ctx and Ltx disassembly, knocking out PDI prevented Ctx and Ltx from intoxicating cells. The absence of a toxin-induced cAMP response in the PDI-deficient cells indicated that PDI-induced toxin disassembly cannot be performed by any other oxidoreductase found in the ER. Interestingly, the PDI-deficient cells were slightly sensitized to Rtx, Stx1, and Stx2 as compared to cells where PDI is fully present. During the knockdown of PDI, it is possible that an upregulation of other oxidoreductases occurs. With an increased level of oxidoreductases to act on these toxins, Rtx, Stx1, and Stx2 could be reduced and disassembled at a higher rate than in the wild-type cells. This would increase the efficiency of A/A1 delivery to the cytosol and produce a sensitizing effect. This also suggests that reduction is a rate-limiting step for intoxication.

Overall, these data suggest that Stx1, Stx2, and Rtx have coupled reduction and disassembly steps, and reduction alone can be performed by any oxidoreductase or reductant. This aids in their ability to move through the ER quickly and reach their cytosolic target to inhibit protein

synthesis. However, disassembly of reduced Ctx and Ltx requires PDI specifically due to its unfolding mechanism for the physical separation of the A1 subunit from $A2/B_5$. These data provide insight to how these AB toxins interact with PDI on a structural level and shed light on a new functionality of PDI that could be exploited for the development of anti-Ctx/Ltx therapeutics.

CHAPTER 3 TOXIN POTENCY IS LINKED TO THE EFFICIENCY OF HOLOTOXIN DISASSEMBLY BY PROTEIN DISULFIDE ISOMERASE

3.1 Introduction

Ctx and Ltx are both AB toxins responsible for causing watery diarrhea in patients and both are known to share ~80% sequence homology [22]. Both toxins bind to the cell surface and are internalized into the endosomes, where they use retrograde transport to move to the ER where they are reduced and disassembled by PDI. After disassembly, the free A1 subunit can then move from the ER into the cytosol where it can reach its cytosolic target, Gsα [16].

Both toxins have a similar structure, move through the cell in a similar fashion, and have the same cytosolic target. However, Ctx is more potent than Ltx in cells [17]. The differential potencies between the two toxins is interesting because Ctx intoxication produces more severe symptoms as compared to a Ltx intoxication [22], and it is unclear why the differential potencies are drastically different.

Both toxins require PDI for disassembly, which can be a rate-limiting step in the intoxication process. Preliminary data show that PDI can more efficiently disassemble Ctx as compared to Ltx (data not shown), which could be responsible for an increase of free CtxA1 subunit in the cytosol as compared to LtxA1. We hypothesize that PDI's disassembly of Ctx and Ltx are rate-limiting, and the efficiency of binding and disassembly dictates toxin potency. Although the structures are similar, the greatest variation between the two toxins resides in the A2 linker region [35]. This region could make it more difficult for PDI to bind to LtxA1 than CtxA1, which would slow the efficiency of Ltx disassembly in comparison to Ctx.

Previous researchers have created chimeric toxins in order to elucidate which region of these toxins dictate toxin potency. Rodighiero *et. al* created holotoxins for wild-type Ctx, wild-type Ltx, and also chimeric toxins which swapped either a section of the A2 linker and the B pentamer, or just the B pentamer [35]. A mutant was also created to determine if the KDEL (Ctx) or RDEL (Ltx) sequences altered the potency of the toxins. All toxins were used to intoxicate cells, and cells were measured by electrical currents to determine the efflux of chloride from the cells. These data showed again that Ctx is more potent than Ltx, but also that chimeras that contained a 10 amino acid segment of the A2 linker and B pentamer from the opposite toxin showed the potency of that toxin: CtxA1/LtxA2/LtxB showed potency similar to wild-type Ltx, and LtxA1/CtxA2/CtxB showed similar potency to wild-type Ctx. Interestingly, switching between the KDEL and RDEL tags did not alter toxin potency [35]. These data demonstrate that the A2 linker, and potentially the B subunit, is responsible for toxin potency, however, the rationale behind this observation is still unknown. We hypothesize that the A2 linker alone is responsible for the change in potency, and the B subunit was utilized to account for the differential C-terminal tails as they entered the central pore.

With the help from our collaborators in Norway, we created mutant Ctx toxins which contained the CtxA1 subunit, point mutations in the CtxA2 sequence that converted it to the LtxA2 sequence, and the CtxB pentamer. These constructs were used in studies to further understand how the A2 linker is involved in the disassembly and potency of Ctx and Ltx. Overall, these data show that the main difference between Ctx and Ltx lies within the A2 linker, and one amino acid change in the A2 linker can drastically alter the potency of the toxin.

3.2 Methods

3.2.1 Nicking of Recombinant Toxins

Recombinant toxins, Ctx, Ltx, CtxV1, and CtxV3, were all produced in *E. coli* and were graciously provided by Dr. Ute Krengel and Joel Heim (Oslo, Norway). Recombinant toxins are not nicked by *E. coli*, and thus need to be first nicked in order to generate a cAMP response. To nick the toxins, toxins (2 μg) were incubated with trypsin (2 μg) for 30 min at room temperature before adding a soybean trypsin inhibitor (4 μg) to inhibit degradation by trypsin. Confirmation of nicking was achieved by running the toxins on a reducing SDS-PAGE to ensure that the toxins were not degraded and were properly nicked, generating a disulfide linked A1/A2 subunit that becomes a smaller molecular weight band when reduced. All toxins were confirmed to be nicked properly before using in intoxication assays.

3.2.2 Ctx Intoxication Assay

CHO cells grown to 80% confluency in 24-well plates were exposed to 10-fold dilutions of Ctx, Ltx, CtxV1, or CtxV3 for 2 h. The cells were then lysed, and data was processed as previously described in Section 2.2.1.

3.2.3 Angle Analysis

With the help of Dr. Tatulian, the angles by which CtxA2 and LtxA2 are positioned with respect to the B pentamers were calculated as described in [36]. The B pentamer plane was established off of leucine 72 in each B subunit monomer, due to its overall stability inside an α-helix, and its availability in both Ctx and Ltx structures.

3.3 Results

3.3.1 Differential Potencies Between Ctx and Ltx

Ctx is more potent than Ltx, however, it is not fully understood why there is differential potency between the two toxins. To establish a baseline of toxin potency between Ctx and Ltx, both toxins were used to intoxicate CHO cells and cAMP was measured (Fig 3.1). Cells exhibited a dose-dependent response to both toxins, however, there was a significant increase in the cAMP levels for cells intoxicated with Ctx as compared to Ltx. Even at the highest concentration, Ltx only exhibited about 50% of the maximal cAMP signal as compared to Ctx. This confirms that Ctx is more potent in cells compared to Ltx, and that our recombinant toxins are functional and mimic the wild type phenotypes for each toxin.

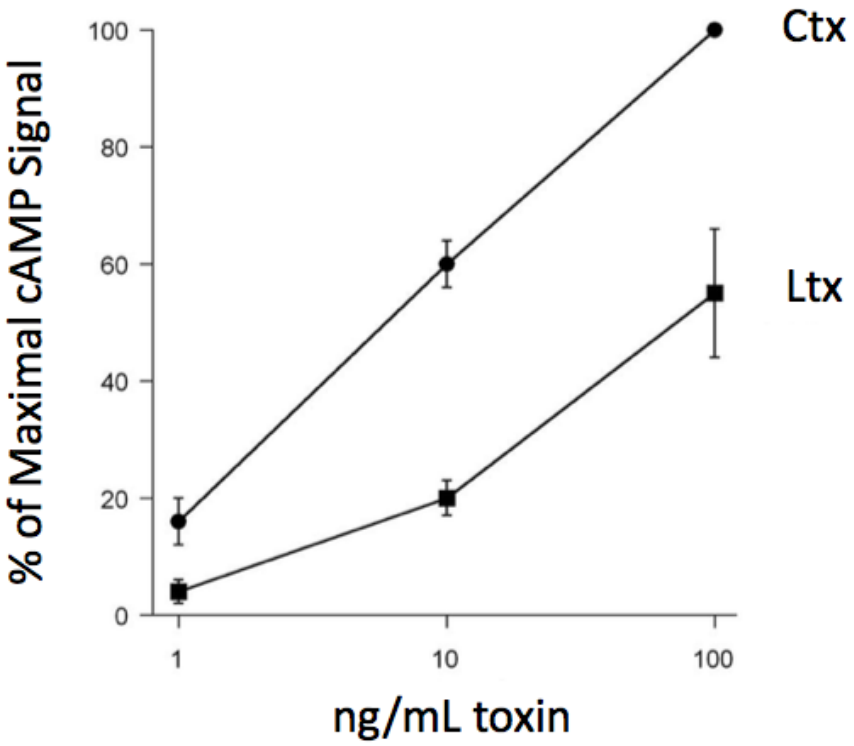

Figure 3.1: Differential Potencies between Ctx and Ltx

CHO cells were intoxicated with increasing concentrations of Ctx (circles) or Ltx (squares) for 2 h before cells were lysed with acidic EtOH. Samples were further processed, and the percentages of cAMP were calculated as a percentage of the maximal cAMP signal, which was Ctx at 100 ng/mL concentration. Samples were done in triplicate, and the experiment was performed six times. Error bars represent the standard error of the mean.

3.3.2 Angle Analysis Between Ctx and Ltx

Ctx and Ltx share ~80% sequence homology, however, the greatest change lies within the A2 linker region of the toxins. The A2 linker is responsible for connecting the A1 subunit to the B pentamer, and the A2 linker is predominately made up of α-helical structure. We hypothesize that the A2 linker is positioning the A1 subunit differently between the two toxins and this could cause a change in how it is disassembled by PDI.

We calculated the angle between the A2 linker and the B pentamer for both wild type toxins from their respective crystal structures and found that the average angle for the entire A2 linker for Ctx was approximately 50^{o}, while the angle for Ltx was approximately 39^{o} (Fig 3.2). In addition to calculating the angles for each toxin, we surprisingly found that the α-helix for both Ctx and Ltx became compromised as the A2 linker entered the central pore of the B pentamer, despite appearing to look α-helical in the crystal structure (data not shown). The initial crystal structure of Ctx (PDB: 1XTC) was used to argue that the tail of the A2 linker remained α-helical and thus provided stability to the overall structure of the holotoxin [37]. Conversely, a later crystal structure of Ctx (PDB: 1S5F) showed a non-helical structure for the tail of the A2 linker, which refuted the idea that this segment is providing stability for the holotoxin [38]. Together, these data demonstrate that there is a significant difference between the two A2 linker regions, and this could be a determining factor in how PDI is able to disassemble the toxins.

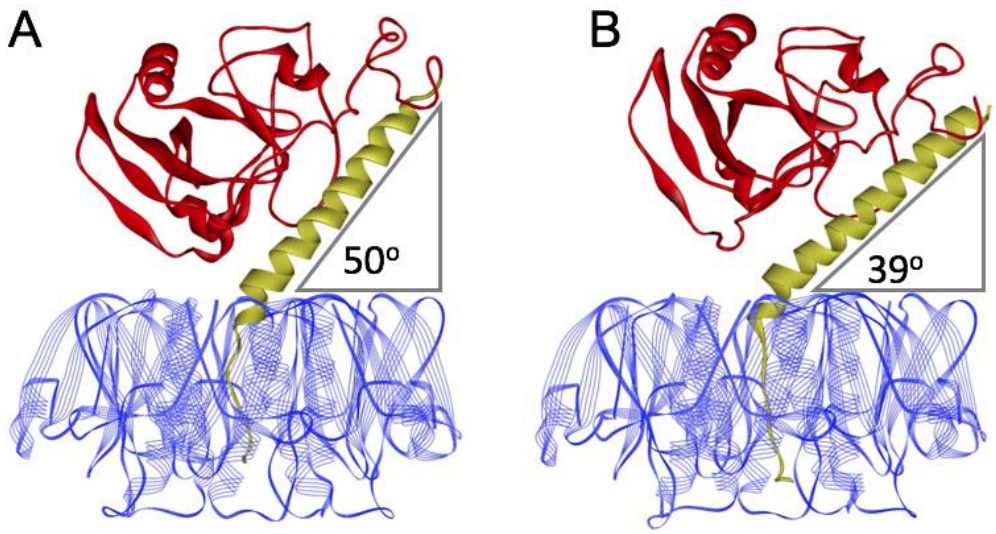

Figure 3.2: Change in A2 linker angle for Ctx and Ltx

Cosines of the α-helical A2 linker relative to the B pentamer were calculated for Ctx (A) and Ltx (B) to determine the change in angle throughout the linker region. The angles of each toxin were averaged to produce an overall angle for the A2 linker. The A1 subunits are shown in red, A2 linker shown in yellow, and B pentamer shown in blue, with the angles of each A2 linker highlighted.

3.3.3 Changes in the A2 Linker Between Ctx and Ltx

The main changes between Ctx and Ltx lie mainly in the A2 linker region, and previous studies have shown that swapping a 10-amino acid segment in the A2 linker between the two toxins alters the toxin potency: Ctx with an LtxA2 segment displayed potency similar to wild-type Ltx, while Ltx with an CtxA2 segment displayed potency similar to wild-type Ctx [35]. We wanted to elucidate the exact amino acids that were responsible for the differential potencies between the toxins, and we were graciously given two mutant Ctxs that had either one amino acid change, or four amino acid changes in the A2 linker that mimic the amino acid found in Ltx at that region. These amino acids, specifically the amino acid at position 229, were chosen because they have been hypothesized to cause a kink in the α-helical linker that begins to exit the B pentamer and could be responsible for creating the angle between the A1 subunit and the B pentamer. A schematic of the amino acid changes can be seen below in Figure 3.3.

To observe differential potencies in the mutant toxins, intoxication assays were performed to see if one or four amino acid changes in the A2 linker caused a significant change in the toxicity of these mutants. KDEL and RDEL tags have been previously shown to have no effect on the differential potency of Ctx and Ltx and were not altered [35]. Cells were intoxicated as previously described with either wild-type Ctx, wild-type Ltx, or with the mutant toxins, CtxV1 and CtxV3 (Fig 3.4). All cells were lysed, processed for cAMP, and compared to the maximal signal, which was Ctx at the highest concentration (100 ng/mL). As shown in Figure 3.4, the two mutant toxins both showed significantly lower cAMP levels as compared to the wild type Ctx. Interestingly, these mutants also showed a similar cAMP response as compared to Ltx, indicating that just one amino acid is responsible for mimicking the Ltx phenotype with a predominately Ctx backbone. This mutant contains wild-type CtxA1 and CtxB, meaning that enzymatic

activity, cell-binding, or intracellular transport are affected by this mutation, and the A2 linker alone is responsible for altering potency. This observation shows that one amino acid change from an aspartic acid at position 229 to a glutamate significantly alters the toxin enough to create a significantly decreased potency.

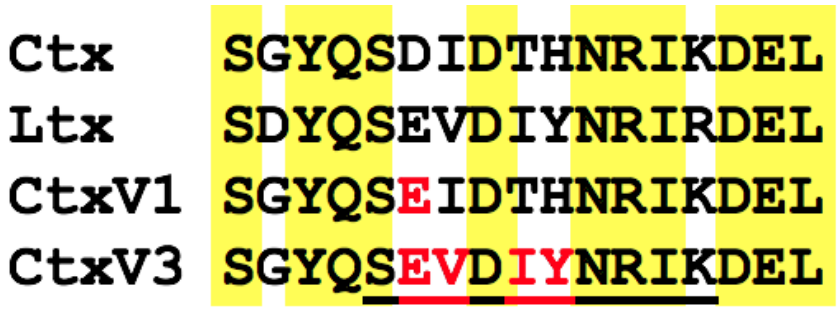

Figure 3.3: Sequence alignment of CtxA2, LtxA2, and Ctx mutants A2 linker

Sequence alignment of the A2 linker region of each of the toxins. The yellow segments show sequence homology between all toxins, where the underlined portion demonstrates the 10-amino acid stretch that was previously switched between toxins by Rodighiero et. al [35]. Amino acids labeled in red were the point mutations to generate the LtxA2 amino acid in the CtxA2 backbone. For CtxV1, one amino acid change was made (D229E), and for CtxV3, four changes were made (D229E, I230V, T232I, and H233Y).

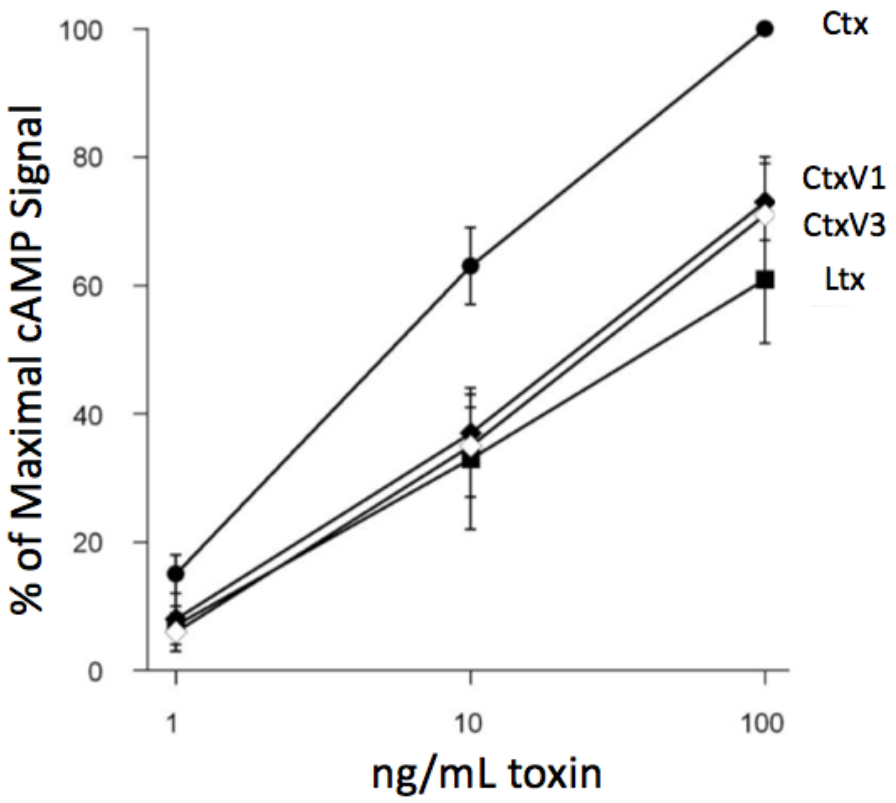

Figure 3.4: Differential potencies between wild type and mutant toxins

Cells were intoxicated with either Ctx (circles), Ltx (squares), CtxV1 (black diamonds), or CtxV3 (open diamonds). 2 h after intoxication, cells were lysed and processed for cAMP. All values are percentages of the maximal cAMP signal, which was Ctx at the highest concentration of 100 ng/mL. All experiments were done in triplicate and repeated 6 times. Error bars represent the standard error of the mean.

3.4 Discussion

Here, we begin to show the key differences between Ctx and Ltx which reside in the A2 linker, and these changes cause a significant structural change between the two toxins. The angle between the A2 linker and the B pentamer could affect how PDI interacts with the holotoxins. It is interesting to note that LtxA1 is a more catalytically active subunit as compared to CtxA1 , so if similar amounts of both subunits were entering the cytosol, then Ltx would create a more robust cAMP response, thus being more potent. However, since this is not the case, we can infer that less LtxA1 is entering the cytosol as compared to CtxA1, leading us to believe that this could be due to the rate at which PDI is disassembling the holotoxin.

While the toxins are very similar, we were able to calculate the average angle of the A2 linker, which showed a 11^{o} change between the two toxins. The change between angles could alter how PDI binds to the holotoxin, and the more acute angle found for the A2 linker of Ltx could be responsible for why PDI is less efficient at binding to and disassembling the holotoxin. It could be that PDI is unfolding and making less contact with the LtxA1 subunit as it does with the CtxA1, thus requiring more force and time for Ltx to be disassembled. Conversely, PDI could have difficulty binding opposite the A2 linker when the angle between the linker and the B pentamer is more acute, causing PDI to take longer to enter the correct space in order for binding to occur, but quickly disassembling the toxin once it is able to bind. Either of these options could be feasible and determining where PDI is binding to these toxins would help us understand how the A2 linker is affecting PDI binding and disassembly.

The creation of Ctx mutants revealed that a single amino acid residue was responsible for changing the toxin potency *in vivo*, which brought new information about how PDI could be affected by the A2 linker. We hypothesize that the single amino acid residue at position 229

could alter the angle of the A2 linker as the α-helix exits the central pore of the B pentamer. Altering this amino acid would alter not only the angle for the A2 linker, but also the toxin potency. Future studies will crystalize the current CtxV1 mutant and calculate the corresponding angle to determine if the angle is similar to Ltx, which would support our hypothesis. Additionally, we intend to model all amino acid substitutions in place of the aspartic acid at position 229. We hope to identify key mutations that produce either no, moderate, or severe changes in the A2 linker angle and produce these toxins to see if they can be disassembled by PDI and by which efficiency. It is possible that these mutations could happen naturally, and because these toxins are inactive, they would have no harmful effect to humans.

Overall, these data have begun to elucidate the main difference between Ctx and Ltx, and how these two toxins differ in potency due to their interaction with PDI. The slight changes in the amino acid chain of the A2 linker provide valuable insight to how these toxins differ structurally, and how these changes can significantly alter the final symptoms in patients. Future work will be dedicated to mapping the binding areas of PDI in both Ctx and Ltx, and the creation of new mutant toxins to further understand how these toxins are interacting with PDI.

CHAPTER 4 QUERCETIN-3-RUTINOSIDE BLOCKS THE DISASSEMBLY OF CHOLERA TOXIN BY PROTEIN DISULFIDE ISOMERASE

4.1 Introduction

Ctx is an AB-type toxin that contains a catalytic A1 subunit and a cell binding B homopentamer, connected by an A2 linker region [22]. Ctx binds to GM1 on the cell surface and is internalized into the endosomes, where it uses retrograde transport to move to the ER for disassembly [34]. Once disassembled, the free A1 subunit can move from the ER to the cytosol, where it can reach its cytosolic target, Gsα, and induce an increase in cAMP [16, 21]. This causes an efflux of water and chloride into the gut, leading to watery diarrhea that affects the approximately 3 million people annually infected with *Vibrio cholerae* [23, 24].

A key step during the Ctx intoxication process is its reduction and disassembly within the ER, and inhibition of these steps prevents Ctx from inducing a cytotoxic effect in cells. The disulfide bond connecting the A1/A2 subunits is first reduced, and then subsequent disassembly occurs during an interaction with PDI, a key oxidoreductase and chaperone found in the ER. PDI disassembles Ctx, and the free A1 subunit, which is unstable at physiological temperatures, spontaneously unfolds [39-41]. The free A1 subunit is then translocated to the cytosol through the ER-associated degradation system, only to evade degradation and reach its target [26, 42, 43].

PDI is known to aid in the reduction and disassembly of Ctx, which are two distinct and separate functions needed to separate the CtxA1 subunit from the rest of the holotoxin. PDI first is capable of reducing the disulfide bond connecting the A1/A2 subunits, and from there PDI can unfold upon binding to Ctx. This unfolding event allows PDI to act as a wedge between the A1

and B subunits and physically dislodges A1 from the rest of the holotoxin [6, 14]. The subsequent, spontaneous unfolding of the free CtxA1 causes PDI to dissociate. It is then able to regain its original conformation.

PDI is required for the disassembly of Ctx, as PDI-deficient cells are resistant to Ctx intoxication. Therefore, inhibition of PDI disassembly could be a potential therapeutic target against Ctx. Better understanding of the unfolding and refolding mechanism of PDI can lead to a better design of potential therapeutics in the future.

PDI contains a U-shaped **abb'xa'c** structural conformation, with 2 active -CGHC- sites in the **a** and **a'** domains, substrate-binding **b** and **b'** domains, a flexible **x** linker, and an acidic **c** region [1, 2]. PDI exhibits two redox-dependent states, where the oxidized state is an open conformation with the **a'** domain being moved out of plane with the rest of the protein by the **x** linker, and the reduced state being a closed, compact conformation with the **a'** domain being in the same plane as the rest of the protein [3, 5, 44]. The changes in PDI's redox state are crucial to substrate binding: PDI can only bind to Ctx in the reduced state, whereas most other substrates, such as insulin, can only bind to PDI in the oxidized form [3, 6, 7]. Due to its flexibility and structural orientation, PDI is able to bind to many substrates in the ER and act as a chaperone and oxidoreductase.

PDI's main functionality has been shown to aid in protein folding in the ER. However, it is also known to circulate in the bloodstream and aid in thrombus formation [45-47]. To find new drugs that prevent blood clot formation, Lin et. al screened a library of compounds and identified a polyphenolic compound, quercetin-3-rutinoside (Q3R), as an inhibitor of insulin reduction by PDI. Q3R also inhibited thrombus formation in mice [48]. The mechanism by which Q3R acts as a PDI inhibitor is still unknown.

Here, we examined the potential use of Q3R as an inhibitor of Ctx. It is known that Q3R blocks some PDI activity and could be used to block PDI during Ctx intoxication. Collectively, we have found that Q3R blocks disassembly of Ctx and protects cultured cells from Ctx intoxication. Additional steps of the intoxication process were also monitored, and Q3R did not show inhibition of PDI binding to CtxA1, toxin reduction by PDI, CtxA1 translocation to the cytosol, or CtxA1 activity in the cytosol. Furthermore, our data indicate that Q3R prevents PDI from undergoing a conformational change during its interaction with Ctx. Therefore, Q3R is inhibiting a key function of PDI which could further be used a potential therapeutic for AB intoxications.

4.2 Methods

4.2.1 Materials

Ctx, CtxA (i.e., the purified CtxA1/CtxA2 heterodimer), Q3R, and PDI were purchased from Sigma-Aldrich (St. Louis, MO). A 35C2 CtxA1 monoclonal antibody was graciously provided by Dr. Holmes [49]. Recombinant PDI was purified as previously described in Section 2.2.5.

4.2.2 Ctx Intoxication Assay

CHO cells grown to 80% confluency in 24 well plates were exposed to 10-fold dilutions of Ctx for 2 h in the absence or presence of 100 µM Q3R. The cells were then lysed and data was processed as previously described in Section 2.2.1.

4.2.3 CtxA1 Transfection Intoxication Assay

CHO cells were transfected with pcDNA3.1/ssCtxA1 [50] using a 3 h incubation with 1 µg of plasmid and LipofectAMINE (Invitrogen, Carlsbad, CA) as the transfection agent. The

transfected cells were then chased in medium lacking or containing 100 µM Q3R. At 4 h post-transfection, cell extracts were generated and processed for cAMP detection as described in Section 2.2.1 for the Ctx intoxication assay. Resting levels of cAMP from mock-transfected cells were background subtracted from the experimental results before presenting the data as percentages of the cAMP response from transfected cells chased in medium lacking Q3R.

4.2.4 Surface Plasmon Resonance (SPR)

A Reichert (Depew, NY) dual-channel SR7000 refractometer with a flow rate of 41 µL/min was used for SPR experiments. To detect PDI binding to CtxA1, His-tagged CtxA1 was appended to one channel of a nickel-nitrilotriacetic acid sensor slide as previously described [6].

To detect PDI-driven Ctx disassembly, the Ctx holotoxin was appended to one channel of a GM1-coated SPR sensor slide as previously described [6]. Perfusion with phosphate-buffered saline containing 0.1% Tween-20 (PBS-T) was used to establish the baseline 0 RIU that corresponded to the mass of the sensor-bound CtxA1 or Ctx. Analyte was then perfused over both channels; the second channel without immobilized ligand was used as a reference cell to account for non-specific binding to the sensor. For the Ctx disassembly assay, sequential additions of anti-PDI (1:10,000 dilution; Enzo Life Sciences, Farmingale, NY), monoclonal 35C2 anti-CtxA144 (1:500 dilution) and anti-CTB antibodies (1:15,00 dilution; Sigma-Aldrich) antibodies were added to the sensor after removing PDI from the perfusion buffer. Control eperiments have previously shown that PDI does not bind to the CtxA2/B_5 complex, that only reduced PDI binds to CtxA1, and that reduction alone is not sufficient for Ctx disassembly [14].

4.2.5 *In Vitro* Toxin Reduction Assay

PDI was incubated with 10 mM GSH for 30 min at room temperature before dialysis with two 1 h exchanges in 1 L PBS. An aliquot of pre-reduced PDI was then treated with a 150-fold molar excess of Q3R for 30 min at room temperature before use. To monitor toxin reduction, 1 µg CtxA was incubated at 37°C for 30 min with 2 µg pre-reduced PDI. Samples were resolved by non-reducing SDS-PAGE with 15% polyacrylamide gels and visualized by Coomassie stain.

4.3 Results

4.3.1 Q3R protects cultured cells from CT

Q3R has been shown to inhibit PDI activity during thrombus formation [45, 51], however, we wanted to know if Q3R-treated PDI would also inhibit Ctx intoxication. To examine this possibility, CHO cells were intoxicated with increasing concentrations of Ctx in the absence or presence of Q3R for 2 h before cAMP levels were measured. As seen in Figure 4.1A, cells intoxicated without Q3R showed an increase of cAMP levels (circles), whereas Q3R treatment reduced the cAMP response to Ctx (squares). Q3R thus protects cultured cells from Ctx.

An alternative toxicity assay demonstrated Q3R did not directly inhibit translocation of the free CtxA1 subunit to the cytosol or the cytosolic activity of CtxA1. For this assay, cells were transfected with a plasmid containing CtxA1 with a signal sequence (ss) that would place it directly into the ER. Upon co-translational entry into the ER, the ss is proteolytically cleaved, leaving the mature CtxA1 subunit which is subsequently translocated back into the cytosol. cAMP levels were recorded 4 h after the end of the transfection. Our results demonstrated Q3R treatment did not affect the cAMP levels when CtxA1 was directly inserted into the ER (Fig

4.1B). Together, the data of Figure 4.1 show that Q3R significantly reduces the Ctx cytotoxicity but does not affect CtxA1 translocation or CtxA1 enzymatic activity.

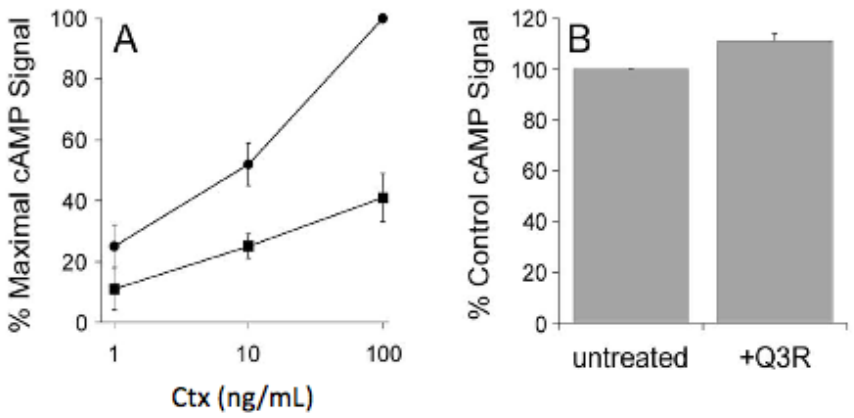

Figure 4.1: Q3R inhibits the cytopathic activity of exogenously applied Ctx but not ER-localized CtxA1

(A) CHO cells were intoxicated with increasing concentrations of Ctx for 2 h in the absence (circles) and presence (squares) of 100 μM Q3R and cytotoxicity was measured by cAMP production. (B) CHO cells transfected with a plasmid containing ssCtxA1 were exposed to 100 μM Q3R for 4 h before measuring cAMP activity. Data are representative of 4 experiments with samples in triplicate, with error bars calculated as the standard error of the mean. All data were expressed as percentages of the maximal (100%) signal, which was the highest cAMP value from intoxicated, non-drug treated cells.

4.3.2 Q3R does not prevent PDI from binding or reducing CtxA1

It is known that Q3R binds to the **b'x** region of PDI [48]**,** which represents its minimum site for binding most substrates. Q3R could block PDI binding to CtxA1, although it is still unknown where PDI binds to CtxA1. We performed two separate binding assays to see if Q3R blocks PDI's ability to bind CtxA1. In the first assay, Q3R-treated PDI was perfused over a CtxA1-coated SPR sensor slide (Fig 4.2A). An increased signal indicated that drug-treated PDI was able to bind to CtxA1. The second assay monitored PDI binding to CtxA1 though the PDI-induced shift in CtxA1 protease sensitivity.CtxA1 is resistant to the thermolysin protease when incubated alone at 30^{o}C but is converted to a protease-resistant state upon binding to PDI [52]. CtxA1 was incubated for 1 h at 30^{o}C in the presence or absence of PDI and Q3R, and then treated with thermolysin on ice for 1 h. All samples were visualized through SDS-PAGE and Coomassie staining. As shown in Figure 4.2B, PDI was capable of putting CtxA1 into a protease-sensitive state when Q3R was present. Q3R alone did not affect CtxA1's protease sensitivity. Together, these data indicate Q3R does not disrupt binding of PDI and CtxA1.

Q3R blocks insulin reduction by PDI, although it is not known if this is due to an inhibition of insulin binding or an inhibition of PDI oxidoreductase activity. PDI was mixed with CTA and visualized with non-reducing SDS-PAGE to see if PDI was capable of reducing the disulfide bond with and without the presence of Q3R. As seen in Figure 4.3, Q3R alone was not capable of reducing the A1/A2 disulfide bond (lane 2), whereas PDI alone (lane 3) or in the presence of Q3R (lane 4) was able to reduce the disulfide, causing a shift from a 27 kDa to a 21 kDa band. This result demonstrated that Q3R does not inhibit reduction of the A1/A2 disulfide bond by PDI.

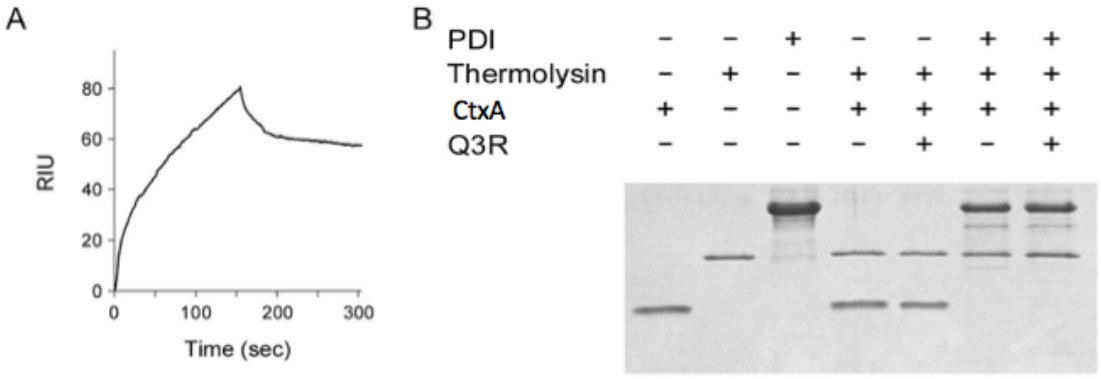

Figure 4.2: Q3R does not affect PDI binding to CTA1

(A) Q3R-treated PDI was perfused over a CtxA1-coated sensor slide which was baselined at 0 RIU. PDI was removed from the perfusion buffer at 150 sec. (B) Various combinations of PDI, thermolysin, CtxA, and Q3R were mixed and incubated for 1 h at 30^{o}C before visualization with SDS-PAGE and Coomassie stain.

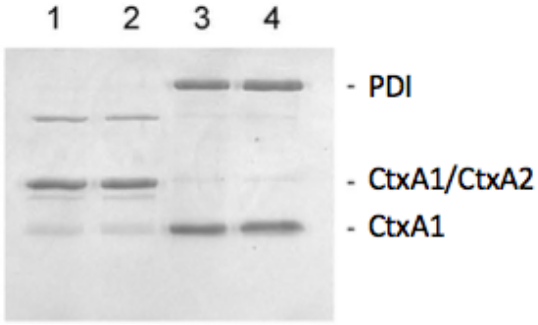

Figure 4.3: Q3R does not affect PDI reduction of the CtxA1/CtxA2 disulfide bond

CtxA was incubated for 30 min at 37°C alone (lane 1), with Q3R (lane 2), with pre-reduced PDI (lane 3), or with pre-reduced PDI treated with Q3R (lane 4). Samples were visualized with non-reducing SDS-PAGE and Coomassie staining.

4.3.3 Q3R disrupts PDI-driven disassembly of the Ctx holotoxin

Q3R does not inhibit PDI binding to CtxA1 or PDI reduction of Ctx, but it does inhibit Ctx intoxication of cultured cells. We accordingly predicted that Q3R blocks the disassembly of Ctx by PDI. SPR was used to observe the PDI-mediated disassembly of Ctx in the presence and absence of Q3R (Fig 4.4). To do this, sensor slides were coated with GM1 to capture the Ctx holotoxin. PDI (Fig 4.4A) or Q3R-treated PDI (Fig 4.4B) were perfused over the slide to allow disassembly, with subsequent antibody controls used to determine what remained bound to the sensor slide (arrowheads). Untreated PDI showed an increased signal indicating binding to Ctx, followed by a drop in signal, showing mass was removed from the slide. Antibody controls showed that PDI was no longer bound and CtxA1 was removed from the plate (Fig 4.4A). Q3R-treated PDI showed a similar initial increase in signal, indicating Q3R-treated PDI bound to Ctx (Fig 4.4B). However, the signal did not drop when Q3R-treated PDI was present and only dropped after PDI was removed. A small portion of PDI did remain bound to the slide, as the signal did not drop back to baseline, and as indicated by the positive signal from the PDI antibody control. Additional antibody controls confirmed that both CtxA and CtxB remained on the slide, meaning no disassembly occurred. The signal dropped when PDI was removed from the perfusion buffer, indicating that PDI dissociated from the slide. These data suggest that Q3R inhibits PDI's ability to disassemble the Ctx holotoxin, even though binding and reduction of the holotoxin are unaffected.

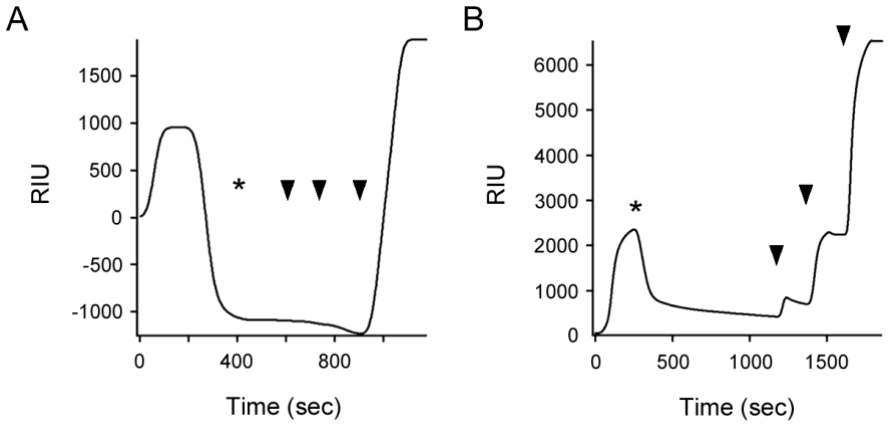

Figure 4.4: Q3R inhibits the PDI-mediated disassembly of Ctx

Ctx was perfused over a GM1-coated sensor slide and baselined to 0 RIU before perfusing over either PDI (A) or Q3R-treated PDI (B). Asterisks indicate when PDI was removed from the perfusion chamber, and arrowheads indicate antibody controls for PDI, CtxA1, and CtxB respectively.

4.3.4 Q3R blocks the conformational change in PDI that occurs with its binding to CtxA1

PDI assumes a compact, rigid structure in the presence of Q3R [48]. This could affect the structural change in PDI that is required for disassembly of the Ctx holotoxin. We examined this possibility with Fourier transform-infrared (FTIR) spectroscopy, a technique that can detect changes in the secondary structure of a protein [53]. As seen in Figure 4.4A, the spectrum of PDI (dashed line) did not shift or change shape in the presence of Q3R (grey line). This indicated that the more compact conformation of Q3R-treated PDI did not alter its global secondary structure. Likewise, Q3R did not affect the overall secondary structure of CtxA1: both untreated (dashed line) and Q3R-treated (grey line) samples of CtxA1 produced nearly identical spectra (Fig 4.4B). We next documented the impact of CtxA1 binding on the structure of PDI (Fig. 4.4C) and examined whether Q3R affected the toxin-induced structural change in PDI (Fig. 4.4D). Uniformly ^{13}C-labeled CtxA1 was used for these experiments in order to distinguish the FTIR spectrum for CtxA1 from the spectrum for PDI. As shown in Figures 4.4C-D and previously reported [6, 54], the spectrum of uniformly ^{13}C-labeled CtxA1 (black lines) exhibited an ~45 cm^{-1} downshift in comparison to the spectrum for unlabeled PDI (grey lines). Adding the spectra from the two individual proteins produced a predicted spectrum for uniformly ^{13}C-labeled CtxA1 and PDI together (blue line). However, this did not match the measured spectrum for the combination of the two proteins in the absence of Q3R (Fig. 4.4C, dashed line). In comparison to the trace of the individual proteins manually added together, there was a significant downshift to the measured spectrum for the combination of uniformly ^{13}C-labeled CtxA1 and PDI. This shift mainly occurred in the 1680-1640 cm^{-1} region that is representative of PDI structure. The opening of PDI tertiary structure in the presence of CtxA1 thus exposed more PDI amino acids to the D_2O buffer, allowing more hydrogen/deuterium exchange for PDI and causing a downshift in

its amide I band to lower frequencies. In contrast, no shift was observed between the predicted (blue line) and measured (dashed line) spectra for the combination of uniformly ^{13}C-labeled CtxA1 and PDI in the presence of Q3R (Fig. 4.4D). This demonstrated that Q3R blocks the CtxA1-induced shift in PDI to a more disordered conformation.

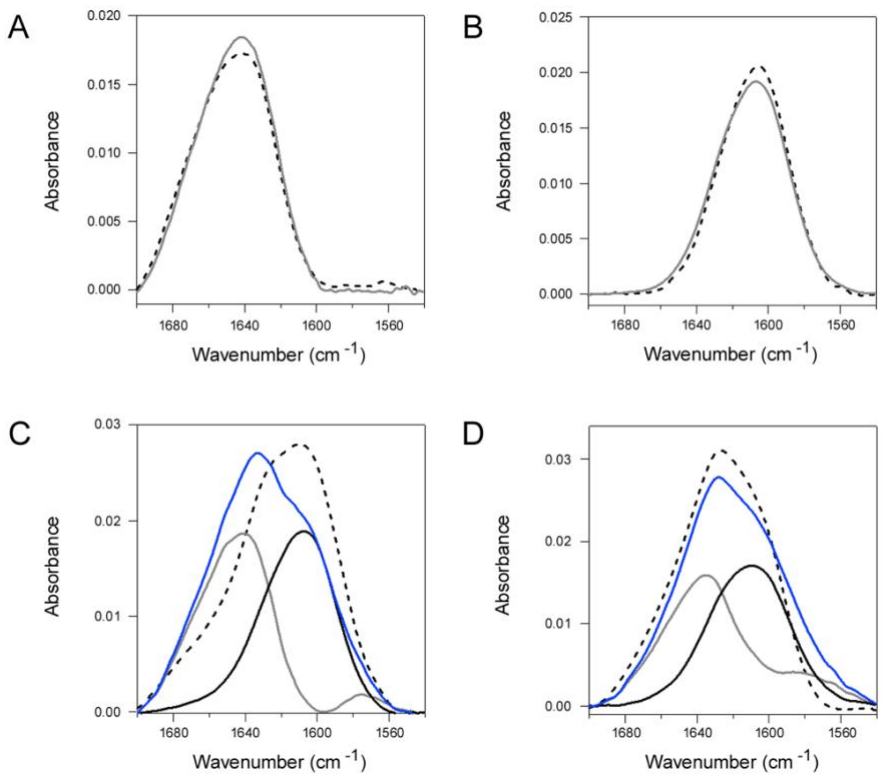

Figure 4.5: Q3R blocks the toxin-induced conformational change in PDI

(A-B) FTIR spectra were recorded for (A) PDI and (B) ^{13}C-labeled CtxA1 alone (dashed lines) or in the presence of Q3R (grey lines). (C) The measured FTIR spectra of PDI alone (grey line) and ^{13}C-labeled CtxA1 alone (black line) were used to generate a predicted spectrum for the combination of PDI and ^{13}C-labeled CtxA1 (blue line). The dashed line presents the measured FTIR spectrum for the combination of PDI and ^{13}C-labeled CtxA1. (D) The measured FTIR spectra of Q3R-treated PDI (grey line) and Q3R-treated, ^{13}C-labeled CtxA1 (black line) were used to generate a predicted spectrum for the combination of PDI and ^{13}C-labeled CtxA1 in the presence of Q3R (blue line). The dashed line presents the measured FTIR spectrum for the combination of PDI and ^{13}C-labeled CtxA1 in the presence of Q3R. All spectra were buffer-subtracted and baselined before comparison, with each experiment performed in duplicate.

4.4 Discussion

Q3R has at least 2 distinct inhibitory effects on PDI. It was originally identified as an inhibitor that blocks insulin reduction and also has been shown to inhibit integrin reduction that initiates thrombus formation [51, 55]. We have shown that it does not block Ctx reduction by PDI, but it does block a conformational change of PDI during its interaction with Ctx.

Q3R occupies the substrate-binding **b'x** region of PDI which could explain its inhibitory effect on substrate reduction. We found that Q3R-treated PDI did not block binding to CtxA1, which was unique considering that it was able to prevent binding to other substrates, such as ricin B chain (data not shown). Previous work has shown that Q3R binds to the **b'x** domain of PDI [48], which could potentially block substrates from binding to that region. It is currently unknown where ricin binds to PDI, and our data suggest that ricin is also binding to the **b'x** domain of PDI, which explains the inhibition of ricin binding to Q3R-treated PDI. In this case, Q3R is acting as a steric inhibitor to ricin B chain, and inhibition of binding subsequently inhibits the reduction of ricin, which is key in preventing ricin disassembly.

Although Q3R and CtxA1 can bind PDI simultaneously, Q3R is still inhibiting PDI from undergoing a conformational change during this interaction. We hypothesize that Q3R is blocking a signal which is being transmitted through the domains to allow unfolding of **a** or **a'**. It is unlikely that either the **b** or **b'** domains are unfolding because PDI has been shown to stay bound to free, folded CtxA1 [6], and loss of the substrate-binding domain would significantly hinder PDI's ability to act on substrates.

In addition to being a steric inhibitor of PDI, Q3R binding could act as an additional stabilizer of the overall structure of PDI. PDI is an extremely flexible protein, with the most flexibility stemming from the **b'x** region, which allows the structural shift between redox states. It is known

that Q3R causes a more compact PDI structure when bound to **b'x** [48], suggesting that Q3R binding to this region could place PDI in a locked conformation and could prevent it from interacting freely with other substrates. This observation, and the notion that Q3R blocks the **b'x** region of substrate binding, together provide new insight into how Q3R is acting as a substrate-specific PDI inhibitor.

PDI is essential for Ctx disassembly and subsequent intoxication because of its unique unfolding property. PDI partially unfolds in the presence of Ctx, and this unfolding acts as a wedge to physically dislodge the A1 subunit from the rest of the holotoxin [14]. This property of PDI has not been seen with other substrates, and it could be dependent on both the redox state of PDI and where the substrate binds to PDI. Q3R prevents the unfolding of PDI and thus blocks the "wedge" mechanism for the disassembly of Ctx. Cells treated with Q3R were thus resistant to Ctx. Both upstream and downstream events of toxin disassembly were not affected by Q3R treatment, indicating that Q3R specifically disrupts PDI's unfolding mechanism and the PDI-mediated disassembly of Ctx. Polyphenolics have been shown to have anti-toxin characteristics, but most of their inhibitory mechanisms are unknown [28, 56, 57]. Here, we provide a molecular mechanism for how Q3R inhibits PDI's interaction with Ctx which could be further used as a potential therapeutic against Ctx intoxication.

CHAPTER 5 CONFORMATIONAL STABILITY AND RESILIENCE OF PROTEIN DISULFIDE ISOMERASE

5.1 Introduction

Protein disulfide isomerase (PDI) is a 57 kDa protein that is predominantly localized to the endoplasmic reticulum (ER) and is required for cell survival [1]. It assists protein folding by acting as both a chaperone and oxidoreductase [8, 9]. These functions are linked to the "U" shape and modular **abb'xa'c** organization of PDI [2, 11]. The **a** and **a'** domains at either end of the U are functional thioredoxin-like domains with conserved -CGHC- regions. The **b** and **b'** domains at the base of the U are inactive thioredoxin-like domains that appear to act as a single unit [58, 59] and are involved with substrate binding, mainly through the **b'** domain [60-62]. The **x** linker is a dynamic, flexible region that facilitates a conformational shift between the oxidized and reduced states of PDI. A short, acidic **c** region at the C-terminus of PDI contains an ER-targeting KDEL motif.

The structure of PDI is affected by its redox state [3, 5]. For the reduced form of PDI (rPDI), the U is a flat structure with all domains in the same plane. This is considered a "closed" conformation because it limits substrate access to the binding domains at the internal base of the U in both human and fungal PDI [4, 63]. For the oxidized form of PDI (oPDI), disulfide bonds connect the cysteine residues within each active site. This is considered an "open" conformation because the **a'** arm is positioned at a ~45° angle away from the plane of the **abb'x** domains. The redox status of PDI thus influences its binding capacity, with most unfolded substrate interactions involving oPDI due to the accessibility of its substrate-binding domain [4, 13, 63-65].

In addition to its redox-sensitive structural change, PDI also exhibits substantial conformational flexibility. Structural studies and molecular dynamics simulations have identified a range of inter-domain movements within PDI [64, 66, 67]. The **bb'** structure is rigid, with limited hinge-like motion and no rotation at the **bb'** interface. The **ab** structure is more flexible, with some hinge-like motion and some rotation at the **ab** interface. The **b'xa'** structure is the most dynamic region, with extensive motional and rotational flexibility. The **a'** domain of rPDI is also more susceptible to proteolysis than the rest of the protein, consistent with its high flexibility [68]. The inter-domain flexibility of PDI, along with intra-domain flexibility in the **b'** domain [64], are key factors that allow PDI to accommodate a wide variety of substrates within its binding pocket at the inner base of the U. Structural analysis of full-length PDI, as well as PDI with whole domain deletions, may therefore shed light on the physical basis of the protein's chaperone function.

The dynamic, redox-dependent nature of PDI influences its interaction with cholera toxin (Ctx). This AB-type protein toxin consists of a catalytic A1 subunit, an A2 linker, and a cell-binding B pentamer [22]. PDI only recognizes the CtxA1 subunit, and only rPDI binds to CtxA1 [6, 7]. Binding occurs after Ctx travels from the cell surface to the ER by retrograde transport [69]. PDI then facilitates the release of CtxA1 from its holotoxin, which is a prerequisite for CtxA1 to enter the cytosol where it elicits a cAMP response through the ADP-ribosylation of Gsα. PDI can reduce the disulfide bond that anchors CtxA1 to CtxA2, but this can also occur at the resident redox state of the ER and does not itself cause holotoxin disassembly [25, 70, 71]. The essential role of PDI in Ctx disassembly instead involves the physical displacement of CtxA1 from its reduced holotoxin [14]. We have shown that rPDI unfolds when it binds to CtxA1 and have proposed the expanded hydrodynamic size of partially unfolded PDI acts as a wedge to dislodge CtxA1 from CtxA2/$CtxB_5$. In support of this model, the inhibition of rPDI unfolding blocks its

disassembly of the reduced Ctx holotoxin without affecting its binding to CtxA1. rPDI returns to a folded conformation after it is released from CtxA1, thereby allowing it to repeat the unfolding process during additional interactions with Ctx. These observations indicate PDI is a resilient protein that can regain a folded, functional conformation after shifting to a disordered state.

To further examine the stability and conformational resilience of PDI, we subjected both rPDI and oPDI to thermal stress. We define conformational resilience as the ability of PDI to refold from a disordered state and consider this to be a linked but distinct phenomenon from its inter-domain conformational flexibility. Our collective data have documented the remarkable redox-dependent conformational resilience of PDI and have identified the contributions of individual PDI domains to its stability. These observations provide new insight into the chaperone function of PDI and its role in stress response.

5.2 Methods

5.2.1 Structural Analysis by CD

Lyophilized proteins (30 µg) were dissolved in 220 µL of 20 mM sodium borate buffer (pH 7.0) containing 100 mM NaCl and, with reduced protein samples, 1 mM DTT. Samples were placed in a 0.1 mm path-length quartz cuvette and read in a Jasco J-1100 CD Spectrophotometer (Jasco Corp., Tokyo, Japan) at various temperatures. Thermal melts were conducted from 20°C to 90°C, with readings taken every 2°C during both heating and cooling back to 20°C. Samples were incubated at each measured temperature for 4 min before measurement. Transition temperatures (T_m) and melt curves were calculated as previously described [26]. For experiments involving transient thermal stress, readings were first taken at 25°C and then 10 min after

incubation at the indicated elevated temperature. A third reading was taken after cooling the sample to 25°C. A baseline reading of buffer alone or buffer with DTT was background subtracted from all protein samples before data analysis. Each sample was read 5 times and averaged to produce the final spectrum from 195-260 nm. After normalizing the traces, data were compiled in Igor (Wavemetrics, Portland, OR) to produce a final figure. A line of best fit was calculated as previously described [26]. All experiments were performed at least twice.

The fraction of unfolded protein at a given temperatute T, f_T, was deduced from the CD spectra using the following formula:

$$f_T = \frac{[\theta]_T - [\theta]_F}{[\theta]_U - [\theta]_F} \qquad (1)$$

where [θ] is the ellipticity at 222 nm and the subscripts T, F, and U indicate the test temperature, a low temperature where the protein is fully folded, and 90ºC where the protein is maximally unfolded, respectively. All calculations were done on individual traces and averaged from duplicate measurements.

5.2.2 Ctx Disassembly Assay

The wells of a 96-well ELISA plate were coated with 6 µg of the Ctx receptor (ganglioside GM1, EMD Millipore, Burlington, MA) in 100% EtOH and left to evaporate overnight. All subsequent additions to the plate were made in phosphate-buffered saline (pH 7.0) with 0.1% Tween 20 (PBS-T) containing 2.5% bovine serum albumin, and all washes were done 4 times with 400 µL of PBS-T. Ctx or CtxB (both from Sigma-Aldrich, St. Louis, MO) were added in 100 ng quantities to each well and incubated at 4ºC for 1 hour. The plate was washed, and 2 µg of PDI was added to each well for 1 h at 37ºC. When indicated, rPDI or oPDI was heated to the

designated temperature for 10 min in a Proflex PCR System (Thermo Fisher Scientific, Waltham, MA) and then allowed to cool for 10 min before addition to the toxin-coated wells. For heated oPDI samples, 1 mM DTT was added to the sample after cooling to place PDI in the proper state for interaction with Ctx. After washing, primary antibody (1:1,000 polyclonal rabbit anti-CtxA, Advanced Targeting Systems, San Diego, CA) was added to the plate for 1 h at 4ºC and washed before adding the secondary antibody (1:1,000 HRP-conjugated goat anti-rabbit IgG, Jackson ImmunoResearch, West Grove, PA) for 30 min at 4ºC. Preliminary experiments confirmed the anti-CtxA antibody recognizes CtxA1 but not the CtxA2 subunit that remains with CtxB after toxin disassembly. After incubation with the secondary antibody, the plate was washed again and blotted dry. TMB substrate (Thermo Fisher Scientific, Waltham, MA) was then added for 5 min before stopping the reaction with 4 N sulfuric acid. Absorbance at 412 nm was read in a BioTek Synergy 2 plate reader (BioTek, Winooski, VT). Values obtained from the CtxB negative control were subtracted from all results before calculating the percentage of toxin disassembly as (1.00 - [PDI-treated Ctx signal / untreated Ctx control signal]) x 100.

5.2.3 Cloning and Purification of PDI Deletion Constructs

The pOLR130 plasmid encoding mature human PDI with an N-terminal His_6 tag [72] was generously provided by Dr. Lloyd Ruddock (University of Oulu, Finland). The **bb'x** construct was cloned from pOLR130 using the primers listed in Table 1. A new vector, pET-His-TEV-LIC encoding mature human PDI, was used as a PCR template to clone the additional PDI deletion constructs with the primers listed in Table 5.1. The pET-His-TEV-LIC vector was cloned from pcDNA3 LIC cloning vector (6A), which was a gift from Scott Gradia (Addgene plasmid # 30124; http://n2t.net/addgene:30124; RRID:Addgene_30124). Insertion of the PCR products into

pET-His-TEV-LIC was performed using the LIC-PCR strategy [73]. The empty plasmid was linearized using Ssp1 and treated, along with the PCR products, with T4 DNA polymerase. The linearized plasmid was then mixed with an individual PCR product to form a closed, complete vector. *E. coli* strain DH5α was transformed with recombinant plasmids and plated overnight. Colonies were selected for plasmid minipreps that were used to confirm the proper coding sequences for our PDI deletion constructs with N-terminal hexahistidine tags. The plasmids were then used to transform *E. coli* strain BL21(DE3)pLysS . Proteins were purified as described in Section 2.2.5.

Table 5.1: Primers (5’ to 3’ orientations) for cloning of the PDI deletion constructs

Construct	Primer	Forward
abb'x	Forward	TACTTCCAATCCAATGCAGACGCCCCCGAGGAG
	Reverse	TTATCCACTTCCAATGTTATTAAGGCTGCTTGTCCCAGTC
bb'x	Forward	TTGGATCCATGCATCACCATCACCATCACATGGCTGCCACCACC
	Reverse	TTGAATTCTTACAGTTCATCTTTCACAGCTTTCTGATCATCGTCTTCC TCCATG TCTGGCTCC
bb'xa'	Forward	TACTTCCAATCCAATGCAGCTGCCACCACCCTG
	Reverse	TTATCCACTTCCAATGTTATTACAGTTCATCTTTCACAGCTTTCTG

5.2.4 FTIR Spectroscopy

CTA1 and/or uniformly ^{13}C-labeled PDI (50 μg each) were dissolved in a D_2O-based buffer containing 20 mM sodium borate and 1 mM GSH, for a total volume of 100 μL. CtxA1 with a C-terminal hexahistidine tag was purified as previously described in Section 2.2.5. All samples were read on a Jasco 4200 FTIR spectrometer (Jasco, Easton, MD) with a Peltier temperature controller (Pike Technologies, Madison, WI). Samples were incubated at either 10°C or 48°C for 5 min before measurements were taken. All traces were baseline corrected and, when necessary, smoothed. Spectral subtraction was used to reveal the gain or loss of amide I components (i.e., respective secondary structures) of PDI resulting from either elevated temperature or interaction with CTA1. Spectral subtractions were preceded by normalization, to obtain similar total intensities of the operand spectra. The spectral ranges for assignment of each secondary structure are as follows: 1690-1660 cm^{-1} for turns, 1659-1646 cm^{-1} for α-helix, 1645-1638 cm^{-1} for irregular structure, and 1637-1620 cm^{-1} for β sheet [74]. The intensity at lower wavenumbers was assigned to side chains. The respective spectral ranges for a ^{13}C-labeled protein were lower by 45 cm^{-1} [14], which accounted for the isotope effect on infrared vibrational frequencies. Final figures showing each individual trace, along with the subtraction of the two comparative traces, were compiled in Igor (Wavemetrics, Portland, OR).

5.3 Results

5.3.1 Thermal Stability of PDI

To establish the thermal stability of PDI, the protein was heated in step-wise fashion from 20°C to 90°C under reducing (1 mM DTT) or oxidizing conditions. A CD spectrum was recorded after

every 2°C increase in temperature, and thermal unfolding profiles were then generated by plotting the ellipticity at 222 nm, $[\theta]_{222}$, versus temperature. Both rPDI (Fig. 5.1A) and oPDI (Fig. 5.1B) produced sigmodial thermal unfolding profiles, but rPDI exhibited a higher transition temperature (T_m) of 54°C than the 48-50°C T_m of oPDI (Table 5.2). A nearly identical T_m of 56°C for rPDI was obtained for a PDI sample pre-treated with 10 mM DTT (not shown). Neither rPDI nor oPDI could fully return to their native conformation after heating over the course of 3 h to 90°C, where the effect of thermal unfolding was saturated. rPDI did regain some of its native structure upon cooling to 20°C, but oPDI did not regain any structure after cooling. Thus, rPDI was more resistant to thermal stress than oPDI.

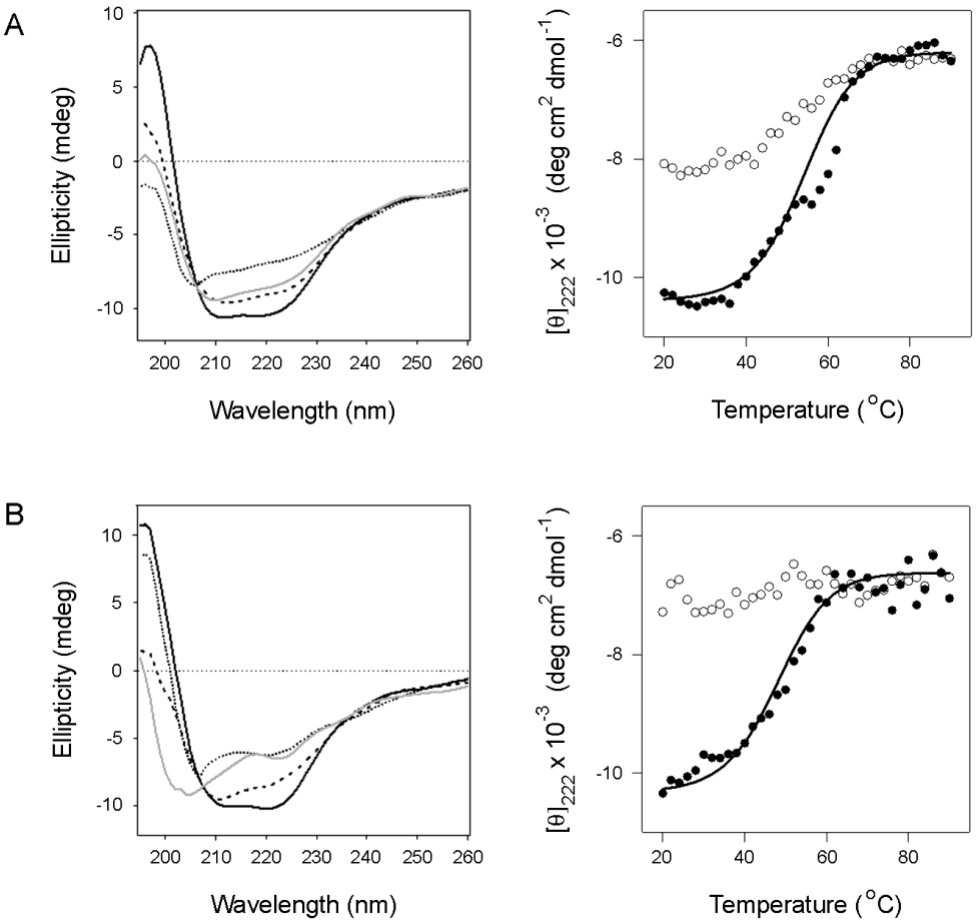

Figure 5.1: Thermal stability of PDI

Reduced (A) or oxidized (B) PDI was heated stepwise from 20°C to 90°C, with CD measurements taken every 2°C. The proteins were then cooled from 90°C to 20°C in the same manner. Representative spectra are shown in the left panels: the initial 20°C measurement (black line) the T_m measurement (dashed line), the 90°C measurement (dotted line), and the final 20°C measurement after cooling (grey line). The right panels plot mean residue molar ellipticities at 222 nm as a function of temperature. Closed circles represent measurements taken during heating; open circles represent measurements taken during cooling.

Table 5.2: Thermal stability of PDI and PDI deletion constructs under reducing or oxidizing conditions

Construct	Reduced	Oxidized
PDI	54°C	48-50°C
bb'xa'c	50-51°C	42°C
abb'x	62-63°C	51-52°C
bb'x	58-60°C	56°C

T_m values representing the ranges of two independent experiments per condition were derived from experiments represented in Figures 5.1 and 5.6.

5.3.2 PDI Resilience and Function After Thermal Stress

To further examine the ability of PDI to refold after thermal denaturation, we rapidly heated rPDI (Fig. 5.2A) or oPDI (Fig. 5.2B) to a set temperature for 10 min before cooling back to 25°C. CD spectra were recorded before heating, after 10 min at the elevated temperature, and after cooling to 25°C. The protocol for thermal denaturation in this experiment was therefore distinct from the prolonged thermal stress used in the experiments of Figure 5.1. For the transient thermal stress, we ran preliminary experiments at several temperatures and chose the minimal temperature that resulted in nearly complete protein denaturation. rPDI only retained 2% of its native α-helical structure after heating to 65°C, yet it regained 85% of its structure after cooling to 25°C (Table 5.2). This demonstrated rPDI could refold from a nearly complete state of thermal denaturation. oPDI exhibited a substantially weaker ability to recover its structure after thermal denaturation, regaining only 62% of its structure after cooling from a 70°C temperature where it maintained even more (12%) of its original structure than the heated rPDI sample (Table 5.3). rPDI thus exhibited a greater propensity for renaturation than oPDI.

Heating rPDI to 90°C for 10 min inhibits its ability to disassemble reduced CT at room temperature [52]. However, it is not known if this loss-of-function is an all-or-none process or if PDI gradually loses function with increasing temperature. To answer this question, an ELISA-based CT disassembly assay was performed after exposing PDI to the thermal stress conditions used in Figure 5.2A-B. PDI was heated and cooled as previously described, and oPDI was then reduced with 1 mM DTT to allow an interaction with CT since only rPDI can bind to CTA1 [6, 7]. All PDI samples were then added to a 96-well plate coated with CT and incubated for 1 h at 37°C to initiate CT disassembly. The release of CTA1 from plate-anchored CTA2/CTB_5 was detected by the loss of signal detected with a primary anti-CTA1 antibody and a secondary

antibody conjugated to horse radish peroxidase (HRP) (Fig. 5.2C). Consistent with previous reports [6, 7, 52], CT disassembly did not occur when oPDI was added in the absence of reductant. CT disassembly by rPDI, which is an inefficient process [7, 52], resulted in a 19% loss of the CTA1 signal. Remarkably, the heat-treated rPDI sample was able to displace CTA1 from CTA2/CTB_5 with greater efficiency than the rPDI control. The gain-of-structure in refolded rPDI thus corresponded to a gain-of-function for its interaction with CT. The oPDI sample that was heated to 70°C and then reduced after cooling could also disassemble CT, but with lower efficiency than the untreated rPDI control. To determine if CT disassembly by oPDI was more efficient after moderate thermal stress, we repeated the disassembly assay with an oPDI sample that was heated to 60°C before cooling, reduction, and addition to CT. This sample of oPDI regained 70 ± 4% of its native structure after 75 ± 5% denaturation (n = 2). Like the heat- treated rPDI sample, this sample of heat-treated oPDI was more effective at CT disassembly than the rPDI control. These data showed that heat-treated PDI is not only functional, but it is able to regain a more active conformation after denaturation from thermal stress.

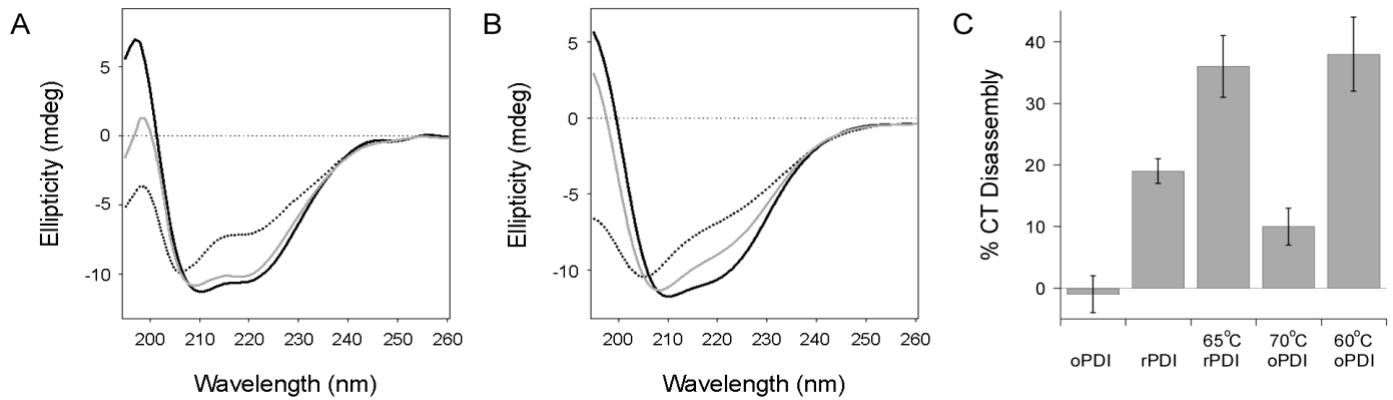

Figure 5.2: Structure and function of refolded PDI

(A-B) CD spectra for rPDI (A) or oPDI (B) were measured at 25°C (black line) before heating rPDI to 65°C and oPDI to 70°C. Spectra were measured again after 10 min at elevated temperature (dotted line) and after cooling back to 25°C (grey line). (C) oPDI and rPDI samples were left at room temperature or heated to the indicated temperatures for 10 min. After cooling to room temperature, each sample was added to a 96-well plate coated with CT. Loss of the CTA1 subunit due to PDI-driven CT disassembly was subsequently detected by ELISA. Final values were calculated based on the maximum CTA1 signal from CT holotoxin incubated in the absence of PDI. Error bars report standard error of the means from at least five independent experiments per condition, each with four replicate samples. All values represent statistically significant differences from the rPDI control (Student's t test, $p < 0.05$).

Table 5.3: Conformational resilience of PDI and PDI deletion constructs under reducing (r) or oxidizing (o) conditions

Construct	Denaturation Temperature	% Folded Structure after Denaturation	% Folded Structure after Renaturation
rPDI	65°C	2 ± 1	85 ± 2
oPDI	70°C	12 ± 4	62 ± 5
r**bb'xa'c**	55°C	12 ± 8	90 ± 0
o**bb'xa'c**	55°C	11 ± 8	90 ± 0
r**abb'x**	65°C	6 ± 6	96 ± 4
o**abb'x**	60°C	14 ± 5	72 ± 8
r**bb'x**	95°C	8 ± 8	74 ± 5
o**bb'x**	70°C	0 ± 0	88 ± 3

The extent of denaturation and renaturation for each construct (± range) was calculated from two independent experiments represented in Figures 5.2 and 5.7.

5.3.3 PDI Refolding After Repeated Transient Stress

Additional CD experiments documented the response of PDI to repeated transient thermal denaturation (Fig. 5.3). PDI was subjected to four sequential rounds of heating and cooling. rPDI generated the same spectrum and returned to the same level of folded conformation (~83% native structure) after each cycle of heating and cooling (Fig. 5.3A). This experiment used the same temperature for rPDI denaturation (65°C) that was used in Figure 5.2. We used 60°C for the repeated thermal stress of oPDI because, as shown in Figure 5.2C, oPDI could return to a fully active conformation after a single 10 min incubation at 60°C but not 70°C. oPDI exhibited a substantially altered structure at the end of the fourth heating/cooling cycle, with a prominent minimum around 208 nm that was not seen in the original spectrum before heating (Fig. 5.3B). Thus, a major difference between rPDI and oPDI is the unique capability of rPDI to regain its initial folded structure after multiple cycles of thermal unfolding and refolding.

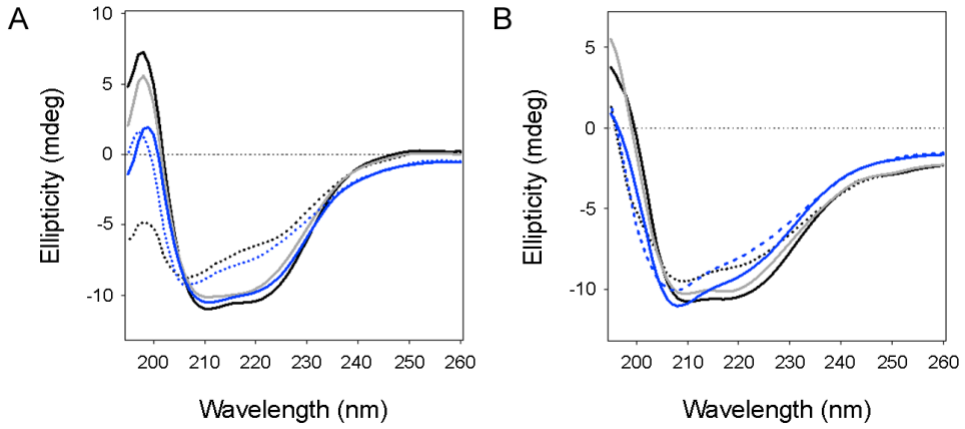

Figure 5.3: Resilience of PDI to repeated thermal stress

CD spectra for rPDI (A) or oPDI (B) were measured at 25°C (black line) before heating rPDI to 65°C and oPDI to 60°C. Spectra were measured again after 10 min at elevated temperature (dotted black line) and after cooling back to 25°C (grey line). The heating/cooling cycle was repeated three times, with the dotted blue lines representing spectra measured at the elevated temperatures of the final (fourth) cycle and solid blue lines representing spectra measured after the final cooling to 25°C.

5.3.4 Similarities Between the Substrate-Induced Unfolding and Thermal Unfolding of PDI

rPDI can refold after substrate-induced unfolding [14] or thermal denaturation (Figs. 5.2-5.3). However, it was unclear whether substrate-induced conformational changes are analogous to those caused by thermal stress. To answer this question, isotope-edited FTIR spectroscopy was used to examine substrate- and temperature-induced changes in the secondary structure of PDI. As shown in Figure 5.4A, the secondary structure of ^{13}C-rPDI was analyzed at 10°C either alone (dashed line) or in the presence of unlabeled CTA1 at 1:1 molar ratio (black line). rPDI does not recognize the disordered conformation of free CTA1 that is present at 37°C, which necessitated the use of low temperature for the measurement of CTA1-bound PDI. For reference, Figure 5.4A also presents the FTIR spectrum of unlabeled CTA1 alone (grey line). These data highlight the expected FTIR spectral shift between the amide I bands of unlabeled and ^{13}C-labeled proteins, which permits evaluation of the structures of both proteins combined in one sample.

To compare the structure of PDI alone with that in the presence of CTA1, the CTA1 spectrum was subtracted from the spectrum of the combined ^{13}C-rPDI / CTA1 sample. This allowed us to resolve the structure of ^{13}C-rPDI during its interaction with CTA1. The resulting spectrum for toxin-treated ^{13}C-rPDI (Fig. 5.4B, dashed line) was broader compared to the spectrum of ^{13}C-rPDI alone (Fig. 5.4B, black line), which was indicative of a more disordered secondary structure of PDI resulting from its interaction with CTA1.

FTIR experiments were conducted, in addition to CD studies, to document the change in rPDI secondary structure resulting from its thermal unfolding. The FTIR spectrum of ^{13}C-rPDI was recorded at 48°C (dashed line) and compared to the 10°C measurement (black line) (Fig. 5.4C). 48°C was chosen for the temperature of thermal unfolding because, based on calculations from the CD thermal melt (Fig. 5.1), the loss of PDI α-helical structure at this elevated temperature

matched the previously reported loss of PDI α-helical structure resulting from its interaction with CTA1 [14]. The spectrum measured at 48°C was broader and shifted to higher wavenumbers compared to the spectrum at 10°C, again indicating a more disordered structure.

We next compared the thermal unfolding of PDI to its CTA1-induced unfolding (Fig. 5.4D). The spectrum of heat-treated ^{13}C-rPDI (Fig. 5.4D, dashed line) was shifted toward higher wavenumbers as compared to CTA1-treated ^{13}C-rPDI (Fig. 5.4D, black line). The difference spectrum (Fig. 5.4D, grey line) indicated a higher fraction of irregular (1604-1595 cm^{-1}) and β-sheet structures (1594-1570 cm^{-1}) in rPDI resulting from its interaction with CTA1 as compared to its partially unfolded structure resulting from thermal stress. This indicated that PDI unfolding caused by its interaction with CTA1 involves a greater loss of α-helical structure than its thermal unfolding, which involves the loss of more β-sheet structure. PDI thus unfolds in distinct ways during thermal stress and upon its interaction with CTA1, yet it can still refold from either disordered state.

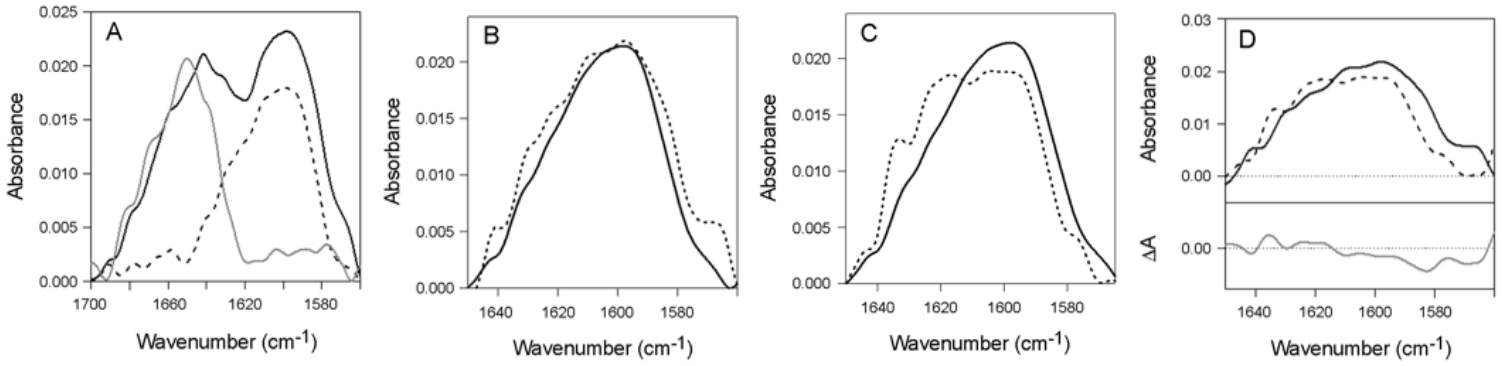

Figure 5.4: Substrate-induced and Thermal Unfolding of PDI

FTIR spectroscopy was used to analyze the secondary structure of rPDI during its interaction with CTA1 or during thermal stress. (A) Spectra of ^{13}C-labeled rPDI (dashed line), unlabeled CTA1 (grey line), and both ^{13}C-labeled rPDI and CTA1 combined at an equimolar ratio (black line) at 10^{o}C. (B) Spectra of ^{13}C-labeled rPDI alone (black line) and ^{13}C-labeled rPDI in the presence of CTA1, with the CTA1 spectrum at 10^{o}C removed (dashed line). (C) Spectra of ^{13}C-labeled rPDI at 10^{o}C (black line) and ^{13}C-labeled rPDI at 48^{o}C (dashed line). (D) Using the data presented in panels B-C, the spectrum for CTA1-treated PDI (black line) was subtracted from the spectrum of heat-treated PDI (dashed line) to generate the difference spectrum (grey line).

5.3.5 Contribution of Individual Domains to the Stability and Conformational Resilience of PDI

We generated PDI deletion constructs that lack either the **a** domain, the **a'** domain, or both **a** and **a'** domains in order to examine how the individual domains of PDI contribute to its overall structural stability. SDS-PAGE was used to confirm the purity of our constructs (Fig. 5.5). Thermal melts were performed in order to determine the stability of each reduced and oxidized construct (Fig. 5.6). We found a **bb'xa'c** deletion construct lacking the **a** domain was less stable than full-length PDI, with a T_m of 50-51°C in the reduced state and 42°C in the oxidized state (Fig. 5.6A, Table 5.2). The oxidized form of **bb'xa'c** also exhibited a distinct thermal melt, with unfolding beginning immediately upon heating from 20°C. In contrast to these results, an **abb'x** deletion construct lacking the **a'c** region was more stable than full-length PDI (Fig. 5.6B, Table 2). The reduced form of **abb'x** exhibited a T_m of 62-63°C, with a sharp transition from its native conformation to its final disordered state. The oxidized form of **abb'x** was substantially less stable than its reduced form, with a T_m of 51-52°C (Fig. 5.6B, Table 5.2). The oxidized forms of **bb'xa'c** and **abb'x** did not regain any structure after cooling from 90°C, while the reduced constructs gained some amount of α-helical structure after cooling. These collective results again demonstrated that the physical properties of PDI are linked to its redox state. Our observations also suggested a stabilizing role for the **a** domain and a destabilizing role for the **a'** domain in the PDI response to thermal stress, which has also been suggested by other investigators [68].
Like **abb'x**, a **bb'x** deletion construct lacking both **a** and **a'** domains was more stable than full-length PDI (Fig. 5.6C, Table 5.2). However, in comparison to **abb'x**, the oxidized and reduced forms of **bb'x** displayed less dramatic differences in stability: reduced **bb'x** exhibited a T_m of 58-

60°C, and oxidized **bb'x** exhibited a 56°C T_m. Given the absence of a disulfide bridge in the **b'** domain of native PDI [4, 75], our results with the reduced form of **bb'x** likely reflect the physiological properties of this PDI region.

To examine how the individual domains in PDI contribute to its overall conformational resilience, each PDI deletion construct was subjected to transient thermal stress under reducing or oxidizing conditions. As previously performed with full-length PDI, we monitored the refolding of each deletion construct after 10 min at the lowest temperature that left the protein in a nearly complete state of denaturation. Heating **bb'xa'c** in either reduced or oxidized forms to 55°C left the deletion construct with 11-12% of its native structure. Upon cooling to 25°C, both reduced and oxidized **bb'xa'c** regained 90% of its native structure (Fig. 5.7A, Table 5.3). This demonstrated that the **a** domain is not essential for the conformational resilience (i.e., refolding) of PDI. Likewise, reduced **abb'x** had only 6% of its native α-helical structure remaining after 10 min at 65°C but regained 96% of its structure upon cooling to 25°C. Oxidized **abb'x** was less resilient than its reduced form, as it only regained 72% of its native structure after heating to 60°C (Fig. 5.7B, Table 5.3). These results indicated both the **a** and **a'** domains can refold after thermal denaturation, with a specific redox-dependent effect on the extent of **a** domain refolding. The **bb'x** construct was less resilient than **bb'xa'c** and reduced **abb'x**, yet it was extremely stable: temperatures of 95°C and 70°C were required for nearly complete denaturation of reduced and oxidized **bb'x**, respectively. These properties were consistent with the rigid nature of **bb'x** [64]. Reduced **bb'x** was able to refold 74% after retaining only 8% of its original structure, while oxidized **bb'x** could refold 88% after retaining none of its native conformation (Fig. 5.7C, Table 5.3). Our collective data suggest **bb'x** confers a high degree of stability to PDI, while both **a** and **a'** domains further contribute to the conformational resilience of PDI.

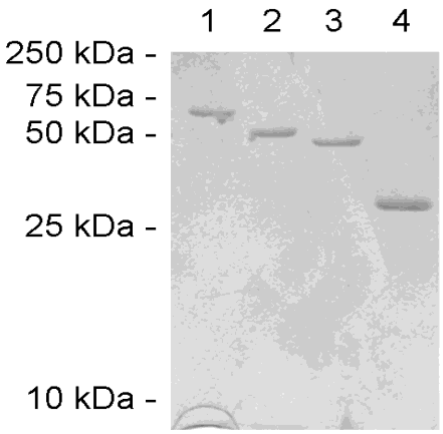

Figure 5.5: Purified PDI constructs

Proteins purified from *E. coli* using TALON affinity chromatrography were visualized on SDS-PAGE with Coomassie stain. Lanes 1-4 contain 2 μg of full-length PDI, **bb'xa'**, **abb'x**, and **bb'x**, respectively. The mobility of molecular mass standards is noted on the left.

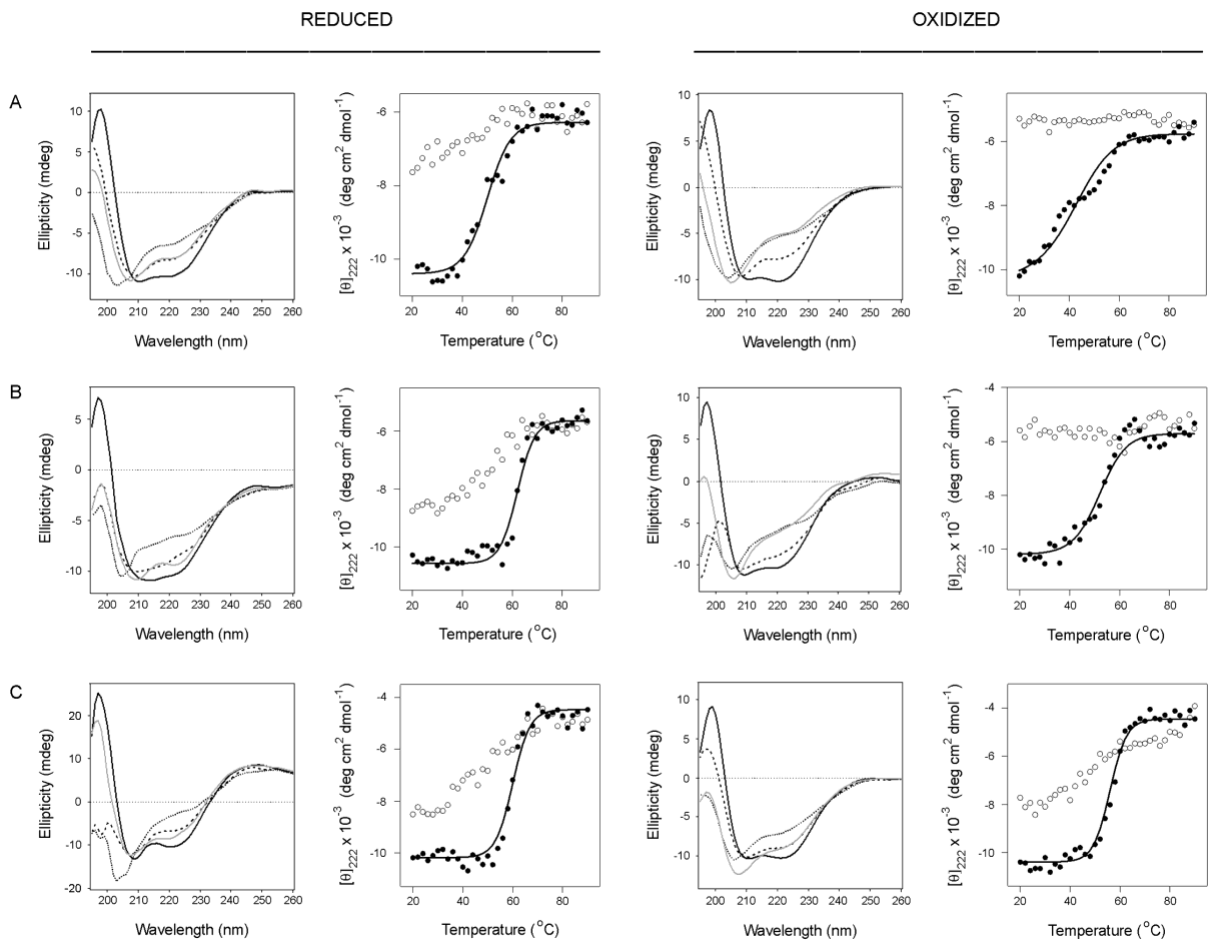

Figure 5.6: Thermal stability of PDI deletion constructs

Reduced or oxidized forms of **bb'xa'c** (A), **abb'x** (B), and **bb'x** (C) were heated stepwise from 20°C to 90°C, with CD measurements taken every 2°C. The proteins were then cooled from 90°C to 20°C in the same manner. Representative spectra are shown in the left panels of each column: the initial 20°C measurement (black line) the T_m measurement (dashed line), the 90°C measurement (dotted line), and the final 20°C measurement after cooling (grey line). The right panels of each column plot mean residue molar ellipticities at 222 nm as a function of temperature. Closed circles represent measurements taken during heating; open circles represent measurements taken during cooling.

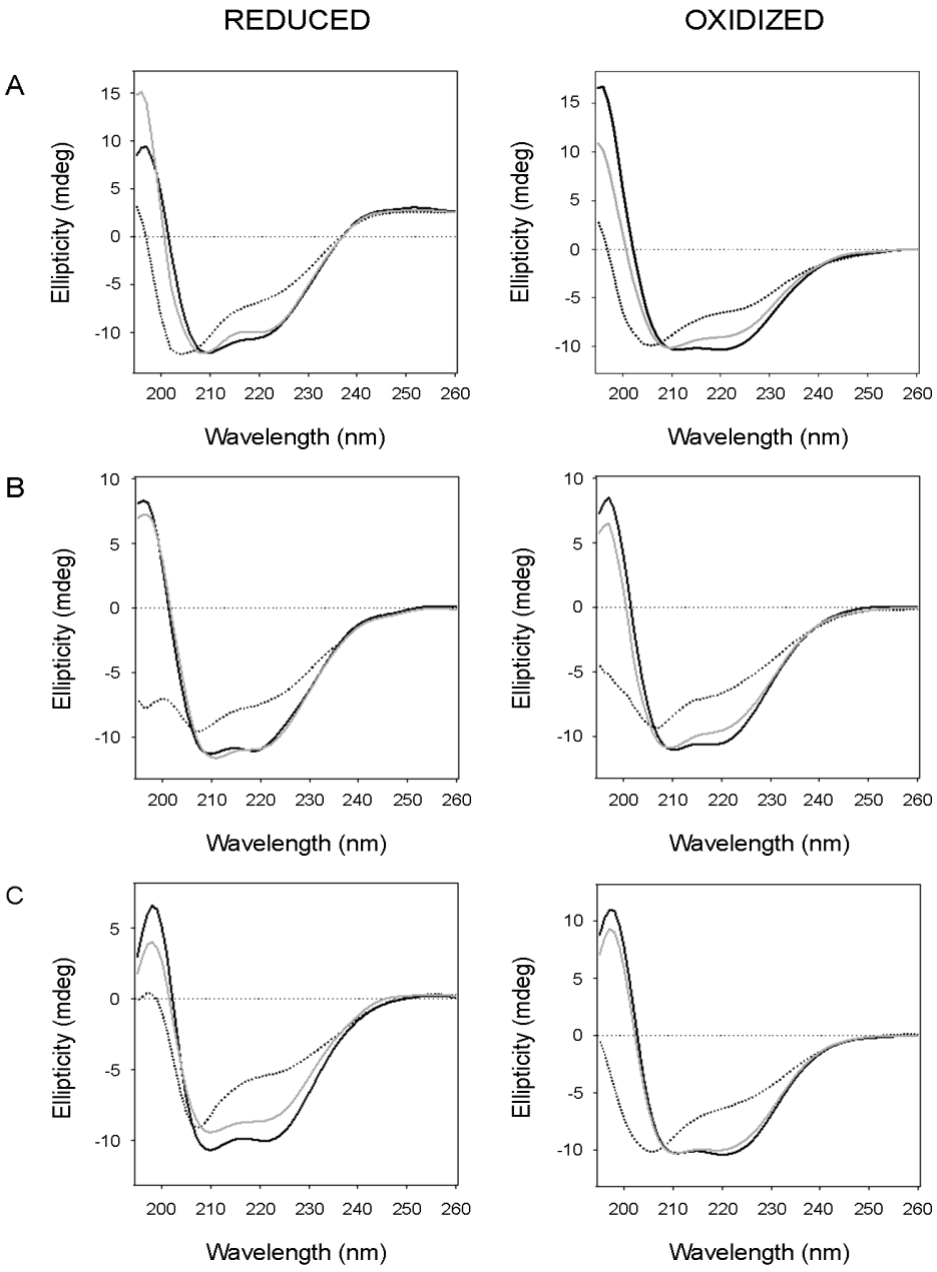

Figure 5.7: Conformational resilience of the PDI deletion constructs

CD spectra for **bb'xa'c** (A), **abb'x** (B), and **bb'x** (C) were measured at 25°C (black line) before heating to temperatures, listed in Table 5.2, that resulted in nearly complete denaturation. Spectra were measured again after 10 min at elevated temperature (dotted line) and after cooling to 25°C (grey line).

5.4 Discussion

The redox-dependent conformational changes to PDI and its conformational flexibility are well-established, but the conformational resilience of PDI has not been examined. Our previous work on PDI-CTA1 interactions documented the ability of PDI to refold after undergoing substrate-induced unfolding [14]. Here, we report that PDI can also return to a functional conformation after thermal denaturation. The conformational resilience of PDI thus appears to derive from a general physical property rather than from a specific, toxin-induced effect. We further document how the functionally important conformational properties of PDI are modulated by its redox state and pinpoint the roles of specific domains in this relationship.

Our data demonstrate that rPDI is substantially more stable and resilient than oPDI. rPDI had a higher T_m than oPDI and, unlike oPDI, could regain some of its native conformation after a thermal melt that exposed it to extreme temperatures for over 3 hours. rPDI was also more resilient to transient thermal stress than oPDI, regaining 85% of its α-helical structure after a 10 min incubation at 65°C left it with just 2% of its native structure. Thus, the redox state of PDI greatly affects both its stability and propensity for renaturation.

We hypothesize the thermal stability of PDI is affected by its flexibility and the dramatic conformational change that occurs between its oxidized and reduced states. rPDI adopts a "closed" conformation in which the **x** linker positions the **a'** domain in line with the rest of the protein [3, 68]. This could stabilize its overall structure, as the **a** and **a'** domains of rPDI are only 27.6 Å apart in the crystal structure, and possibly even closer in soluble PDI [3, 65, 67]. Conversely, the “open” conformation of oxidized PDI positions the **a'** domain at a 45° angle away from the protein core. This separates the **a** and **a'** domains by 40.3 Å in the crystal structure

of PDI. The expanded structure of oPDI would likely have fewer inter-domain contacts than rPDI, which is consistent with fungal PDI [76], and would therefore be less stable than rPDI. The deletion constructs provided insight regarding which PDI domains contribute to its physical properties. The **bb'x** core of PDI confers a high degree of stability to PDI, which is consistent with the rigid nature of this region [64]. The **a** and **a'** domains of PDI appear to play opposing roles in its thermal stability, with a stabilizing role for the **a** domain and a destablizing role for the **a'** domain. Full-length PDI is less stable than the **abb'x** deletion construct, which indicates the **a** domain cannot completely compensate for the destablizing effect of the **a'** domain. In contrast to their differing roles in stability, both the **a** and **a'** domains appear to facilitate the conformational resilience of PDI as demonstrated by the extensive refolding of both **abb'x** and **bb'xa'c** deletion constructs after their nearly complete denaturation. However, **bb'xa'c** exhibited a redox-independent response to transient thermal stress: the minimal temperature required for denaturation and the extent of refolding after denaturation were identical for both oxidized and reduced **bb'xa'c**. This redox-independent response was unique to **bb'xa'c**, which suggests the conformational resilience of PDI is regulated by oxidation of the **a** domain.

The ER-localized pool of PDI exists in an equilibrium between its oxidized and reduced states, and these levels are in dynamic equilibrium due to the oxidoreductase activity of PDI [10]. oPDI assists oxidative protein folding by creating and rearranging disulfide bonds in exchange for reducing its own. rPDI can then interact with additional substrates such as CTA1, or it can regenerate its active site disulfide bonds through an interaction with either Ero1p or oxidized glutathione [77, 78]. Previous studies have determined about 15% of the ER-localized pool of PDI is oxidized [79], which indicates a large pool of stable, rPDI is consistently available to

withstand stress conditions. This pool of PDI would likely remain functional after ER stress and could thus help rapidly restore homeostasis to the ER.

The conformational resilience of PDI may also play a direct role in its chaperone activity. We have suggested the unfolding/refolding cycle PDI exhibits in its interaction with CT represents a normal property of PDI that could be used to disrupt protein aggregates in the same way its substrate-induced unfolding leads to the physical displacement of CTA1 from the CT holotoxin [14]. In support of this hypothesis, we found a transient thermal stress that resulted in the nearly complete denaturation of PDI did not prevent it from returning to a functional conformaton that could still disassemble CT (Fig. 5.3). In fact, our data suggest the unfolding/refolding cycle may actually enchance PDI-driven CT disassembly. Repeated substrate interactions that lead to the unfolding and refolding of PDI could thus prime its chaperone-linked ability to block or possibly reverse protein aggregation. It should be noted, however, that PDI is not currently known to act as a disaggregase for any substrate. Further examination of this hypothesis will require the identification of an appropriate aggregation-prone substrate for the chaperone activity of PDI.

CHAPTER 6 CONCLUSION

This body of work documents the molecular mechanism of how PDI interacts with five different AB toxins, and how these interactions lead to differential toxin potencies. PDI is capable of reducing the disulfide bond for the toxins tested. However, only Ctx and Ltx require PDI's unique unfolding mechanism to allow disassembly. This disassembly event is crucial in determining the differential potencies between toxins, and it can be utilized as a potential target for future anti-toxin therapeutics.

AB toxins must be first reduced and then disassembled to be toxic in cells [18, 19]. We have shown that reduction and disassembly are coupled events for Rtx and Stx, which we attribute to their structurally open conformations that ensure there is nothing left to hold the holotoxin together once reduction occurs, thus allowing the separation of the A or A1 subunits from the rest of the holotoxin. Conversely, both Ctx and Ltx have more compact structures, and reduction alone does not lead to the disassembly of these toxins. Once the disulfide bond is broken between the A1 and A2 subunits, the closed structure allows non-covalent forces to hold the holotoxin together as one unit, and disassembly cannot occur until these forces have been overcome.

Since reduction alone is sufficient for Rtx and Stx disassembly, we have shown that multiple oxidoreductases and reductants are capable of disassembling these toxins, and PDI is not essential for their intoxication. Since PDI is not a rate-limiting step in their cellular activities, it could explain why both Rtx and Stx are extremely potent toxins as compared to Ctx and Ltx. We have demonstrated that Ctx produces a higher cAMP response as compared to Ltx when cells are intoxicated with the same concentrations of toxin, although LtxA1 is known to have higher

activity as compared to CtxA1. These data suggest that more Ctx is being disassembled and more CtxA1 is entering the cytosol as compared to Ltx.

Due to their structural differences, Ctx and Ltx have more compact structures and require an extra step during their disassembly process as compared to Rtx and Stx. We have shown that PDI is required for the disassembly of these toxins because of its unfolding mechanism which provides the extra force to overcome the non-covalent bonds holding the reduced holotoxin together. Other oxidoreductases or reductants can reduce Ltx but are incapable of removing the A1 subunit from the rest of the holotoxin, so cells deficient in PDI are resistant to both Ctx and Ltx intoxications. Blocking the PDI unfolding mechanism is key to blocking Ctx and Ltx *in vivo*, but blocking this action will still allow intoxication of Rtx and Stx.

Q3R was found during a screen of PDI inhibitors when testing its ability to reduce insulin, but the mechanism of action remains unknown. Surprisingly, Ctx was still able to bind and become reduced by Q3R-treated PDI, indicating that Ctx could be binding in a different region of PDI as compared to insulin [48]. Furthermore, the disaggregase activity of PDI was also inhibited by Q3R, thus allowing cells to become resistant to Ctx intoxications. Interestingly, Q3R has previously been shown to compact PDI's structure, and this compaction could be inhibiting PDI from unfolding during its interaction with Ctx or Ltx. We hypothesize that CtxA1/LtxA1 binding to the **b** domain sends a signal through the **b'x** domains to allow the **a'** domain to unfold during this substrate-induced unfolding event. Addition of Q3R could block the signal from traveling to the **a'** domain, preventing it from unfolding upon binding to Ctx or Ltx. The flexibility of PDI can also be altered during its interaction with Q3R, which could significantly alter PDI's overall stability and resilience as a protein.

PDI has demonstrated high levels of conformational stability and resilience, and this resilience is what allows PDI to unfold and refold during its interaction with Ctx and Ltx. PDI was shown to have increased stability and resilience when in the reduced state, which is the same state that is able to bind to and interact with the AB toxins that were tested. This ability to unfold and refold has been utilized by these toxins in order to exhibit toxic effects, however, PDI's resilience and stability indicate that this could be a normal function of PDI used to break apart protein aggregates in cells. Our lab has demonstrated that PDI is capable of breaking apart nascent fibrils of α-synuclein, which eventually create plaques in neurons and can lead to Parkinson's disease. This new property of PDI needs to be fully explored to understand which substrates activate the disaggregase activity in PDI, and how this can be utilized to break apart protein aggregates commonly found in neurodegenerative diseases.

Overall, this dissertation explores the interaction between PDI and various AB toxins, and how these interactions dictate toxin potency. It also sheds light on a new functionality of PDI that was previously unknown. These data are key in fully understanding how PDI interacts with its substrates, and how PDI has the potential to be utilized for anti-toxin therapeutics and treatments to protect against neurodegenerative diseases.

LIST OF REFERENCES

1. Turano, C., et al., *Proteins of the PDI family: unpredicted non-ER locations and functions.* J Cell Physiol, 2002. **193**(2): p. 154-63.

2. Kozlov, G., et al., *A structural overview of the PDI family of proteins.* FEBS J, 2010. **277**(19): p. 3924-36.

3. Wang, C., et al., *Structural insights into the redox-regulated dynamic conformations of human protein disulfide isomerase.* Antioxid Redox Signal, 2013. **19**(1): p. 36-45.

4. Wang, C., et al., *Human protein-disulfide isomerase is a redox-regulated chaperone activated by oxidation of domain a'.* J Biol Chem, 2012. **287**(2): p. 1139-49.

5. Wang, L., X. Wang, and C.C. Wang, *Protein disulfide-isomerase, a folding catalyst and a redox-regulated chaperone.* Free Radic Biol Med, 2015. **83**: p. 305-13.

6. Taylor, M., et al., *Protein disulfide isomerase displaces the cholera toxin A1 subunit from the holotoxin without unfolding the A1 subunit.* J Biol Chem, 2011. **286**(25): p. 22090-100.

7. Tsai, B., et al., *Protein disulfide isomerase acts as a redox-dependent chaperone to unfold cholera toxin.* Cell, 2001. **104**(6): p. 937-48.

8. Bulleid, N.J. and L. Ellgaard, *Multiple ways to make disulfides.* Trends Biochem Sci, 2011. **36**(9): p. 485-92.

9. Ali Khan, H. and B. Mutus, *Protein disulfide isomerase a multifunctional protein with multiple physiological roles.* Front Chem, 2014. **2**: p. 70.

10. Margittai, E., et al., *Composition of the redox environment of the endoplasmic reticulum and sources of hydrogen peroxide.* Free Radic Biol Med, 2015. **83**: p. 331-40.

11. Appenzeller-Herzog, C. and L. Ellgaard, *The human PDI family: versatility packed into a single fold.* Biochim Biophys Acta, 2008. **1783**(4): p. 535-48.

12. Kanemura, S., et al., *Human ER Oxidoreductin-1alpha (Ero1alpha) Undergoes Dual Regulation through Complementary Redox Interactions with Protein-Disulfide Isomerase.* J Biol Chem, 2016. **291**(46): p. 23952-23964.

13. Hatahet, F. and L.W. Ruddock, *Protein disulfide isomerase: a critical evaluation of its function in disulfide bond formation.* Antioxid Redox Signal, 2009. **11**(11): p. 2807-50.

14. Taylor, M., et al., *Substrate-induced unfolding of protein disulfide isomerase displaces the cholera toxin A1 subunit from its holotoxin.* PLoS Pathog, 2014. **10**(2): p. e1003925.

15. Sandvig, K. and B. van Deurs, *Delivery into cells: lessons learned from plant and bacterial toxins.* Gene Ther, 2005. **12**(11): p. 865-72.

16. Beddoe, T., et al., *Structure, biological functions and applications of the AB5 toxins.* Trends Biochem Sci, 2010. **35**(7): p. 411-8.

17. Mukhopadhyay, S. and A.D. Linstedt, *Retrograde trafficking of AB(5) toxins: mechanisms to therapeutics.* J Mol Med (Berl), 2013. **91**(10): p. 1131-41.

18. Cho, J.A., et al., *Insights on the trafficking and retro-translocation of glycosphingolipid-binding bacterial toxins.* Front Cell Infect Microbiol, 2012. **2**: p. 51.

19. Odumosu, O., et al., *AB toxins: a paradigm switch from deadly to desirable.* Toxins (Basel), 2010. **2**(7): p. 1612-45.

20. Spooner, R.A. and J.M. Lord, *Ricin trafficking in cells.* Toxins (Basel), 2015. **7**(1): p. 49-65.

21. Sanchez, J. and J. Holmgren, *Cholera toxin - a foe & a friend.* Indian J Med Res, 2011. **133**: p. 153-63.

22. Julie E. Heggelund, V.A.B., Ute Krengel, *Vibrio cholerae and Escherichia coli heat-labile enterotoxins and beyond*, in *The Comprehensive Sourcebook of Bacterial Protein Toxins*. 2015.

23. Hsiao, A., et al., *The health economics of cholera: A systematic review.* Vaccine, 2018. **36**(30): p. 4404-4424.

24. Wierzba, T.F., *Oral cholera vaccines and their impact on the global burden of disease.* Hum Vaccin Immunother, 2018: p. 1-8.

25. Majoul, I., D. Ferrari, and H.D. Soling, *Reduction of protein disulfide bonds in an oxidizing environment. The disulfide bridge of cholera toxin A-subunit is reduced in the endoplasmic reticulum.* FEBS Lett, 1997. **401**(2-3): p. 104-8.

26. Pande, A.H., et al., *Conformational instability of the cholera toxin A1 polypeptide.* J Mol Biol, 2007. **374**(4): p. 1114-28.

27. Yermakova, A., et al., *Neutralizing Monoclonal Antibodies against Disparate Epitopes on Ricin Toxin's Enzymatic Subunit Interfere with Intracellular Toxin Transport.* Sci Rep, 2016. **6**: p. 22721.

28. Friedman, M. and R. Rasooly, *Review of the inhibition of biological activities of food-related selected toxins by natural compounds.* Toxins (Basel), 2013. **5**(4): p. 743-75.

29. Shi, W.W., et al., *Structures and Ribosomal Interaction of Ribosome-Inactivating Proteins.* Molecules, 2016. **21**(11).

30. Olsnes, S., et al., *Immunotoxins--entry into cells and mechanisms of action.* Immunol Today, 1989. **10**(9): p. 291-5.

31. Basu, D. and N.E. Tumer, *Do the A subunits contribute to the differences in the toxicity of Shiga toxin 1 and Shiga toxin 2?* Toxins (Basel), 2015. **7**(5): p. 1467-85.

32. Strockbine, N.A., et al., *Cloning and sequencing of the genes for Shiga toxin from Shigella dysenteriae type 1.* J Bacteriol, 1988. **170**(3): p. 1116-22.

33. Garred, O., et al., *Role of the disulfide bond in Shiga toxin A-chain for toxin entry into cells.* J Biol Chem, 1997. **272**(17): p. 11414-9.

34. Lencer, W.I., et al., *Targeting of cholera toxin and Escherichia coli heat labile toxin in polarized epithelia: role of COOH-terminal KDEL.* J Cell Biol, 1995. **131**(4): p. 951-62.

35. Rodighiero, C., et al., *Structural basis for the differential toxicity of cholera toxin and Escherichia coli heat-labile enterotoxin. Construction of hybrid toxins identifies the A2-domain as the determinant of differential toxicity.* J Biol Chem, 1999. **274**(7): p. 3962-9.

36. Tatulian, S.A., *Determination of helix orientations in proteins.* Comput Biol Chem, 2008. **32**(5): p. 370-4.

37. Zhang, R.G., et al., *The three-dimensional crystal structure of cholera toxin.* J Mol Biol, 1995. **251**(4): p. 563-73.

38. O'Neal, C.J., et al., *Crystal structures of an intrinsically active cholera toxin mutant yield insight into the toxin activation mechanism.* Biochemistry, 2004. **43**(13): p. 3772-82.

39. Taylor, M., D. Curtis, and K. Teter, *A Conformational Shift in the Dissociated Cholera Toxin A1 Subunit Prevents Reassembly of the Cholera Holotoxin.* Toxins (Basel), 2015. **7**(7): p. 2674-84.

40. Banerjee, T., et al., *Contribution of subdomain structure to the thermal stability of the cholera toxin A1 subunit.* Biochemistry, 2010. **49**(41): p. 8839-46.

41. Surewicz, W.K., J.J. Leddy, and H.H. Mantsch, *Structure, stability, and receptor interaction of cholera toxin as studied by Fourier-transform infrared spectroscopy.* Biochemistry, 1990. **29**(35): p. 8106-11.

42. Massey, S., et al., *Stabilization of the tertiary structure of the cholera toxin A1 subunit inhibits toxin dislocation and cellular intoxication.* J Mol Biol, 2009. **393**(5): p. 1083-96.

43. Teter, K. and R.K. Holmes, *Inhibition of endoplasmic reticulum-associated degradation in CHO cells resistant to cholera toxin, Pseudomonas aeruginosa exotoxin A, and ricin.* Infect Immun, 2002. **70**(11): p. 6172-9.

44. *Human protein-disulfide isomerase is a redox-regulated chaperone activated by oxidation of domain a'.* 2012. **287**(2): p. 1139-49.

45. Chiu, J., et al., *Protein Disulfide Isomerase in Thrombosis.* Semin Thromb Hemost, 2015. **41**(7): p. 765-73.

46. Cho, J., *Protein disulfide isomerase in thrombosis and vascular inflammation.* J Thromb Haemost, 2013. **11**(12): p. 2084-91.

47. Schulman, S., et al., *Extracellular Thiol Isomerases and Their Role in Thrombus Formation.* Antioxid Redox Signal, 2016. **24**(1): p. 1-15.

48. Lin, L., et al., *Quercetin-3-rutinoside Inhibits Protein Disulfide Isomerase by Binding to Its b'x Domain.* J Biol Chem, 2015. **290**(39): p. 23543-52.

49. Holmes, R.K. and E.M. Twiddy, *Characterization of monoclonal antibodies that react with unique and cross-reacting determinants of cholera enterotoxin and its subunits.* Infect Immun, 1983. **42**(3): p. 914-23.

50. Teter, K., M.G. Jobling, and R.K. Holmes, *Vesicular transport is not required for the cytoplasmic pool of cholera toxin to interact with the stimulatory alpha subunit of the heterotrimeric G protein.* Infect Immun, 2004. **72**(12): p. 6826-35.

51. Flaumenhaft, R. and B. Furie, *Vascular thiol isomerases.* Blood, 2016. **128**(7): p. 893-901.

52. Cherubin, P., et al., *Protein disulfide isomerase does not act as an unfoldase in the disassembly of cholera toxin.* Biosci Rep, 2018. **38**(5).

53. Tatulian, S.A., *Structural analysis of proteins by isotope-edited FTIR spectroscopy.* Spectroscopy Int. J., 2010. **24**(1-2): p. 37-43.

54. Taylor, M., et al., *Substrate-induced unfolding of protein disulfide isomerase displaces the cholera toxin A1 subunit from its holotoxin.* PLoS Pathogens, 2014. **10**(2): p. e1003925.

55. Furie, B. and R. Flaumenhaft, *Thiol isomerases in thrombus formation.* Circ Res, 2014. **114**(7): p. 1162-73.

56. Cherubin, P., et al., *Inhibition of Cholera Toxin and Other AB Toxins by Polyphenolic Compounds.* PLoS One, 2016. **11**(11): p. e0166477.

57. Reddy, S., et al., *Grape extracts inhibit multiple events in the cell biology of cholera intoxication.* PLoS One, 2013. **8**(9): p. e73390.

58. Denisov, A.Y., et al., *Solution structure of the bb' domains of human protein disulfide isomerase.* FEBS J, 2009. **276**(5): p. 1440-9.

59. Karamzadeh, R., et al., *Machine Learning and Network Analysis of Molecular Dynamics Trajectories Reveal Two Chains of Red/Ox-specific Residue Interactions in Human Protein Disulfide Isomerase.* Sci Rep, 2017. **7**(1): p. 3666.

60. Hatahet, F. and L.W. Ruddock, *Substrate recognition by the protein disulfide isomerases.* FEBS J, 2007. **274**(20): p. 5223-34.

61. Klappa, P., et al., *The b' domain provides the principal peptide-binding site of protein disulfide isomerase but all domains contribute to binding of misfolded proteins.* EMBO J, 1998. **17**(4): p. 927-35.

62. Cheung, P.Y. and J.E. Churchich, *Recognition of protein substrates by protein-disulfide isomerase. A sequence of the b' domain responds to substrate binding.* J Biol Chem, 1999. **274**(46): p. 32757-61.

63. Yagi-Utsumi, M., T. Satoh, and K. Kato, *Structural basis of redox-dependent substrate binding of protein disulfide isomerase.* Sci Rep, 2015. **5**: p. 13909.

64. Freedman, R.B., et al., *'Something in the way she moves': The functional significance of flexibility in the multiple roles of protein disulfide isomerase (PDI).* Biochim Biophys Acta Proteins Proteom, 2017. **1865**(11 Pt A): p. 1383-1394.

65. Serve, O., et al., *Redox-dependent domain rearrangement of protein disulfide isomerase coupled with exposure of its substrate-binding hydrophobic surface.* J Mol Biol, 2010. **396**(2): p. 361-74.

66. Romer, R.A., et al., *The flexibility and dynamics of protein disulfide isomerase.* Proteins, 2016. **84**(12): p. 1776-1785.

67. Yang, S., et al., *Compact conformations of human protein disulfide isomerase.* PLoS One, 2014. **9**(8): p. e103472.

68. Wang, C., et al., *Plasticity of human protein disulfide isomerase: evidence for mobility around the X-linker region and its functional significance.* J Biol Chem, 2010. **285**(35): p. 26788-97.

69. Wernick, N.L.B., et al., *Cholera toxin: an intracellular journey into the cytosol by way of the endoplasmic reticulum.* Toxins, 2010. **2**(3): p. 310-325.

70. Mekalanos, J.J., R.J. Collier, and W.R. Romig, *Enzymic activity of cholera toxin. II. Relationships to proteolytic processing, disulfide bond reduction, and subunit composition.* J Biol Chem, 1979. **254**(13): p. 5855-61.

71. Orlandi, P.A., *Protein-disulfide isomerase-mediated reduction of the A subunit of cholera toxin in a human intestinal cell line.* J Biol Chem, 1997. **272**(7): p. 4591-9.

72. Nguyen, V.D., et al., *Two endoplasmic reticulum PDI peroxidases increase the efficiency of the use of peroxide during disulfide bond formation.* J Mol Biol, 2011. **406**(3): p. 503-15.

73. Aslanidis, C. and P.J. de Jong, *Ligation-independent cloning of PCR products (LIC-PCR).* Nucleic Acids Res, 1990. **18**(20): p. 6069-74.

74. Tatulian, S.A., *Structural characterization of membrane proteins and peptides by FTIR and ATR-FTIR spectroscopy.* Methods Mol Biol, 2013. **974**: p. 177-218.

75. Nguyen, V.D., et al., *Alternative conformations of the x region of human protein disulphide-isomerase modulate exposure of the substrate binding b' domain.* J Mol Biol, 2008. **383**(5): p. 1144-55.

76. Nakasako, M., et al., *Redox-dependent domain rearrangement of protein disulfide isomerase from a thermophilic fungus.* Biochemistry, 2010. **49**(32): p. 6953-62.

77. Kulp, M.S., et al., *Domain architecture of protein-disulfide isomerase facilitates its dual role as an oxidase and an isomerase in Ero1p-mediated disulfide formation.* J Biol Chem, 2006. **281**(2): p. 876-84.

78. Wang, L., et al., *Reconstitution of human Ero1-Lalpha/protein-disulfide isomerase oxidative folding pathway in vitro. Position-dependent differences in role between the a and a' domains of protein-disulfide isomerase.* J Biol Chem, 2009. **284**(1): p. 199-206.

79. Appenzeller-Herzog, C. and L. Ellgaard, *In vivo reduction-oxidation state of protein disulfide isomerase: the two active sites independently occur in the reduced and oxidized forms.* Antioxid Redox Signal, 2008. **10**(1): p. 55-64.